This is to certify that the

thesis entitled

EFFECT OF SPARK PLUG GROUND
ELECTRODE GEOMETRY ON EXHAUST
EMISSIONS OF SMALL UTILITY ENGINES

presented by

Mahmood Ahmed Akhter Rahi

has been accepted towards fulfillment
of the requirements for

M.S. degree in Mechanical Engineering

Major professor

Date 5/13/98.

O-7639

PLACE IN RETURN BOX to remove this checkout from your record.
TO AVOID FINES return on or before date due.
MAY BE RECALLED with earlier due date if requested.

DATE DUE	DATE DUE	DATE DUE

EFFECT OF SPARK PLUG GROUND ELECTRODE GEOMETRY ON EXHAUST EMISSIONS OF SMALL UTILITY ENGINES

By

Mahmood Ahmed Akhter Rahi

A THESIS

Submitted to
Michigan State University
In partial fulfillment of the requirements
For the degree of

MASTER OF SCIENCE

Department of Mechanical Engineering

1998

ABSTRACT

EFFECT OF SPARK PLUG GROUND ELECTRODE GEOMETRY ON EXHAUST EMISSIONS OF SMALL UTILITY ENGINES

By

Mahmood Ahmed Akhter Rahi

With increasingly stringent regulations placed on exhaust emissions of small utility engines, more opportunities for reduction in emissions are being explored. This thesis presents the results of a study in which the influence of spark plug electrode shape on exhaust emissions of three small utility engines is analyzed. The spark plugs studied were Champion models of standard electrode shape and spark plugs with a crown-shaped electrode, believed by the manufacturer (Pyrotek) to give improved combustion.

The experimental results indicate that the Pyrotek spark plug causes an appreciable reduction in hydrocarbon emissions with a moderate increase in emissions of oxides of nitrogen. The Pyrotek plug was more sensitive to changes in the angular position of the ground electrode, spark gap, engine speed, and to minor changes (i.e. notches) to the electrode's geometry. The reduction in hydrocarbon emissions is attributed to a faster burning rate and flame front propagation. The Pyrotek plug is also thought to favor the formation of more spherical flame fronts than the baseline spark plug and to influence the bulk charge motion in the vicinity of the spark gap.

This thesis is dedicated to my parents

Bashir Ahmed Akhter (late)

&

Salima Akhter

For their love, kindness and prayers for my success

ACKNOWLEDGMENT

I would like to pay special thanks to a few important people:

First, I would like to extend my sincere gratitude to Dr. Giles Brereton, my Major Professor, for being my adviser, and for his support and patient guidance throughout my thesis work and studies.

Dr Harold Schock, for being on my committee, and for his moral support and guidance; Dr Indrek Wichman, for being on my committee and for his helpful attitude and guidance in understanding the peculiar nature of the problem; Dr Keunchel Lee and Dr Bassam Ramadan for their valuable comments; Lawrence Dalimonte for his help in setting up the engines and data collection; Tom Stueken, for his help in test rig modification and professional photography. I would also like to thank my fellows at MSUERL, for their day to day guidance and their wonderful company; Matt Foster, Jon Darrow, Mark Novak, Mikhail Ejakov and Hans Hascher.

Finally, my wife Rashda, for her patience and support throughout my Masters Program, and my mother without whose prayers, this day would not have been possible.

TABLE OF CONTENTS

LIST OF TABLES

LIST OF FIGURES

NOMENCLATURE

English Symbols

Name	Meaning	Units
A	Area	cm^2
A_f	Flame surface area	cm^2
A_c	Contact area between the flame front and electrode	cm^2
$Bm, B\phi$	Parameters of equation (24)	*cm/s*
b	Combustion chamber bore	*m*
C	Capacitance	*Farad*
c	Speed of sound	*m/ sec*
C_i	Constant specific to the engine	--
E	Energy discharged	*Joules*
E_a	Activation energy	*J/Kmole*
E_{ign}	Minimum ignition energy	*J*

hc	Enthalpy of combustion or enthalpy	J/Kg
h	Hight of the combustion chamber	m
K	Stretch factor	--
$l0$	Integral scale or Taylor macro scale	m
$m^{\bullet}$	Mass flow rate	kg/sec
$m^{\bullet'''}$	Volumetric mass production rate	$Kg/s\text{-}m^3$
Ma	Markstein Number	--
$Q^{\bullet'''}$	Volumetric energy generation rate	W/m^3
R	Radius or specific gas constant	m or $J/Kg\text{-}K$
R_{crit}	Critical radius	m
Rf	Flame kernel radius	m
S_l	Laminar flame speed	m/s
S_t	Turbulent flame speed	m/s
T	Temperature	K
u'	Turbulence intensity	--
V	Voltage	$volts$
V	Volume	m^3
W	Volumetric mass consumption rate	$Kg/m^3\text{-}s$
Y_R	Mass fraction of reactants	Kg/Kg

Greek Symbols

α	Thermal diffusivity	m^2/s
β	Pressure exponent	--

δ	Laminar flame thickness	*m*
ϕ	Equivalence ratio	--
ϕ_m	Parameter defined in Equation (23)	--
γ	Temperature exponent	--
λ	Thermal conductivity	*W/m-K*
θ	Crank angle	*Degrees*
θ_0	Crank angle at start of combustion	*Degrees*
$\Delta\theta$	Total combustion duration in crank angle	*Degrees*
ρ	Density	Kg/m^3
ρ_u	Unburned gas density	Kg/m^3
ρ_b	Burned gas density	Kg/m^3
$\rho_{u,ign}$	Unburned gas density at the time of ignition	Kg/m^3
τ	Characteristic burn time	*Sec*

<u>Acronyms</u>

AFR	Air Fuel Ratio	Kg_{air}/Kg_{Fuel}
CO	Carbon Monoxide	--
CO_2	Carbon Dioxide	--
COV	Coefficient of Variance	--
HC	Hydrocarbon	--
IMEP	Indicated Mean Effective Pressure	N/m^2
NO_x	Oxides of Nitrogen	--
OHV	Overhead Valve	--

SI	Spark ignition	--
TDC	Top Dead Center	--
UHC	Unburned hydrocarbons	--
VLV	Vector Lightweight Vertical	--
WOT	Wide Open Throttle	--

CHAPTER I

INTRODUCTION

1.1 Overview

The performance levels required of gasoline engines have been rising with each passing year. Recently, attention has been focused on factors improving performance and emissions in small utility Spark Ignition (SI) engines, with trends towards the use of catalytic converters, leaner air/fuel ratios, etc. In the case of the smaller utility engines, which tend to operate at rich air-fuel ratios, the exhaust-gas emissions remain a major cause for concern. For reference purposes, typical values of SI exhaust emissions from an automotive engine are given at Table 1[1].

Table 1: Typical Levels of Exhaust Emissions for Automotive SI Engines

Pollutant	Emissions(kg/1000 liters)
Aldehydes	0.5
Carbon monoxide *(CO)*	276
Hydrocarbons *(HC)*	24
Oxides of Nitrogen *(NO_x)*	14
Particulate	1.4
Organic Acids	0.5
Sulfur oxides	1.1

In engine combustion, the first important stage of the combustion process is the ignition. In many investigations conducted to date, attempts have been made to improve combustion in the engines by enhancing ignition. Using more energetic sparks in the engine's ignition system can reduce exhaust emissions and fuel consumption. Enhancement of ignitability depends on a large number of parameters such as: spark energy, mixture composition, initial pressure and temperature, oxidation kinetics and bulk fluid motion in the vicinity of spark gap.

In this study, the performance of the Pyrotek spark plug (with a crown-shaped ground electrode geometry) relative to a Champion spark plug (baseline) was compared in terms of exhaust emissions. The Champion spark plug is representative of all baseline spark plugs because the geometry of the ground electrode is essentially identical to all the other brands. The comparison was made by carrying out a series of laboratory experiments, in which engines operated at the same controlled conditions were tested first with one spark plug, then the other.

The effectiveness of each spark plug was measured in several engines in terms of changes in hydrocarbon and NO_x emissions. In general, increases in NO_x emissions correspond to increases in burning rate as a consequence of a larger initial flame kernel. It has been observed experimentally that larger initial flame kernels cause higher burning rates, torque and NO_x emissions, and lower the hydrocarbon emissions [20].

The hydrocarbon emissions are mainly due to flame quenching in crevices. A faster reaction causes higher flame temperatures with higher NO_x emissions. However, higher heat losses may lower the relative NO_x emissions. The mechanism of formation of these noxious emissions is discussed in the following section.

1.2 Formation of Noxious Exhaust Emissions

1.2.1 Carbon Monoxide

At the high temperatures and pressures during the combustion process, significant quantities of CO form, even when there is sufficient oxygen for complete combustion to occur. This CO formation is due to a dissociation reaction, which can lead to equilibrium compositions of the products of combustion having significant CO at high temperatures. The majority of the rate equations involved in the CO formation and oxidation to CO_2 proceed sufficiently fast that equilibrium occurs within a few crank-angle degrees.

Once the exhaust valve opens, measurements indicate [1] that the rapid fall in pressure and temperature, due to exhaust blow down, may cause some departure from equilibrium. However, the reaction rates for the above process are fast enough that, even here, equilibrium is maintained. As the mixture becomes richer, the CO concentration increases at a progressively faster rate and rapidly becomes quite significant due to insufficient oxygen to complete the combustion. Therefore, final CO formation is predominantly controlled by the equivalence ratio.

1.2.2 Unburned Hydrocarbons

Most of the initial unburned hydrocarbons exist in the quench zone. The quench zones are defined as the regions where the flame can not be supported. Crevice regions such as the space above the upper piston ring and within the spark plug (area between insulator nose and internal seal) are the important quench areas, but some quench areas exist adjacent to walls of the combustion chamber, on account of wall heat transfer and their inhibition of flame-front propagation. In addition, unburned hydrocarbons result from absorption and desorption of unburned fuel from engine oil at the cylinder wall during a single cycle.

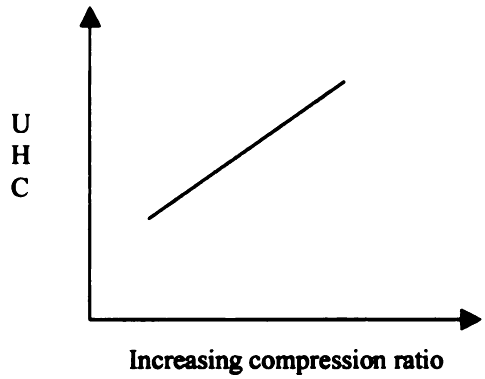

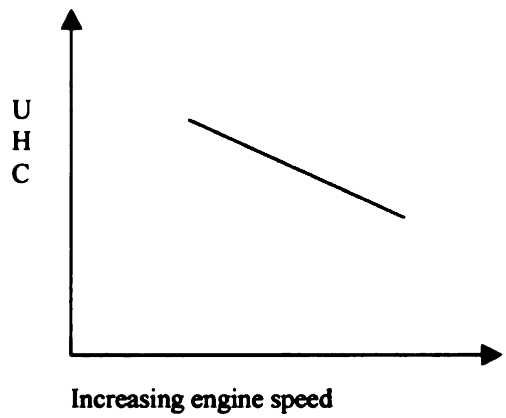

Figure 1: Trends in Hydrocarbon Emissions with Variation in Engine Parameters [1]

Unburned hydrocarbons from within the quench regions in engines are expelled during the exhaust process. The lowest levels of unburned hydrocarbons tend to occur at an equivalence ratio slightly less than one. The major engine variables affecting the unburned hydrocarbons in SI engines are equivalence ratio, compression ratio, engine speed, and spark timings.

A higher compression ratio increases unburned hydrocarbons because, with a smaller combustion space at Top Dead Center (TDC), the quench zone comprises a larger proportion of the total volume. Unburned hydrocarbons decrease with increasing engine speed because the correspondingly higher turbulence levels promote faster combustion and decrease the size of the quench zone. In the case of a retarded spark, the unburned hydrocarbons decrease because more combustion occurs after TDC, when the combustion volume is enlarging and the quench zone is proportionally smaller. Moreover, retarding the spark results in exhaust gases at higher temperatures so that more oxidation of *HC* can take place in the exhaust system.

1.2.3 Oxides of Nitrogen

The formation of oxides of nitrogen is a highly temperature dependent phenomenon. It occurs because equilibrium concentrations of various NO_x compounds form when oxygen and nitrogen are mixed at high temperatures such as 2000°K to 3000°K. However, the reaction rates are slow relative to engine-combustion time scales and equilibrium is not fully attained in the time available under most engine conditions. This applies, to some extent, to the forward reaction but is particularly true of the backward reaction.

$$O + N_2 \Leftrightarrow NO + N \tag{1}$$

The NO_x is effectively frozen for a long period after it is exhausted from the engine, giving it time to react with other substances to form photochemical smog. The rate of NO_x formation is also coupled to the levels of turbulence in the flow. At peak combustion temperatures, small changes in temperature correspond to large differences in the amount of NO_x formed. This is predominantly due to the observation that combustion is faster at higher turbulence levels and reaches higher peak temperatures[1].

1.2 Literature review

It is a well-known observation that the geometric details of the spark plug electrodes affect ignition and early flame growth processes. There has been very little quantification of this observation. In a spark ignition engine, one is interested in the effectiveness of the spark plug in igniting a mixture and ensuring a faster burn rate. Many studies have been carried out to gauge the mixture ignitabilities as measures of spark-plug performance. One of the methods used by Daniel and Scilzo [2] was to measure the Coefficient of Variance (COV) of Indicated Mean Effective Pressure (IMEP) at idle and lean fuel conditions. Nishio, Oshima, Kyongdoung and Heywood [3] have used Air to Fuel (A/F) ratio lean limit as the lean limit comparison test, to determine the leanest mixture that can be ignited by a spark plug. Hood [4] used the counting method to count lean limit misfires during a certain interval of time, in order to determine which spark plug shows a better performance in terms of igniteability. In addition, maximum Exhaust Gas Recirculation (EGR) tolerance has also been used as a parameter to measure the ignitability by the spark plug.

Piston motions in engines impose constraints on ignition and flame propagation via pressure and temperature in the end gas on the one hand and charge motion and turbulence on the other. Maly, Saggau, Wagner and Ziegler [11], while evaluating the prospects of ignition enhancement, concluded that these constraints may be overcome by improved ignition devices, which provide the largest possible expansion velocities and initial sizes of the flame kernel.

Brereton, Bertrand and Macklem, [13] while evaluating the effects of changing humidity and temperature on the emissions of small utility engines, noticed the strong influence of varying humidity on *HC* emissions. Hadjiconstantinou, Kyoungdoug and Heywood [5] correlated the flame propagation characteristics with hydrocarbon emissions. They concluded that mean engine hydrocarbon emission levels increased when the air to fuel ratio increased above its stoichiometric value because of decreasing *HC* oxidation. Furthermore, they noticed that for stoichiometric mixtures, there was no correlation between the individual cycle burn rate and *HC* emissions because changes in the flame speed and exhaust gas temperature cancelled each other.

Mantel [21] showed that in the presence of a mean velocity field, the development and propagation of the flame depended largely on the flow field induced by the ground electrode in the vicinity of and particularly in the wake of the spark gap. Bianco, Cheng and Heywood [6] characterized the behavior of the flame kernel by an expansion speed which describes its growth rate, and a convection velocity, which describes its overall movement.

Herweg, Begleris, Zettlitz, and Zeilger [8] used high speed Schlieren photography in an optically accessible side chamber and found that the flame kernel is changed by the turbulence at flame radii of 0.5 to 1 mm, depending on turbulence intensity. The influence of turbulence on the turbulent burning velocity during the flame kernel formation is less compared to the main combustion period. Hall [9] noticed that turbulence of higher intensity and smaller scale enhances the rate of flame kernel growth, even for relatively young flames (having a diameter of up to 1 cm), and for mixtures having an equivalence ratio as lean as 0.7.

A number of studies have been conducted on the effect of ground electrode orientation. Anderson and Asik [25] found experimentally that the orientation of the conventional spark plug ground electrode, with respect to the mean swirl velocity, can have a quantifiable effect on combustion stability and average burn time. Positioning the ground electrode upstream of the oncoming swirl flow resulted in improved flame initiation over a downstream, or 180 degree rotated position. Zeigler, Schaudt, and Herweg [26] found improved flame initiation with the ground electrode positioned dowstream of a uniform in a flow combustion chamber.

Witze [7] investigated the effect of the spark plug location on the burning rates with a disc shaped combustion chamber. He deduced that, in general, ignition at the center of the chamber was preferable. While evaluating the effect of spark duration on combustion, Nakai, Nakagawa, Hamai, and Sone [12] found that lengthening the spark duration helped to promote flame kernel growth. This was attributed to the continued supply of spark energy to the flame kernel as it is being formed during the initial stage of ignition.

Heat losses from the spark-ignited flame kernel to the electrode play an important role in SI engine combustion. Pischinger and Heywood [24] had deduced from experiments using high speed photography that the heat losses from the electrodes can promote cycle to cycle variations in the initial flame kernel growth. The heat losses vary from cycle to cycle, due to substantial cycle to cycle variation in the contact area between the flame kernel and the electrodes. Anbarasu and Abata [10] investigated the effect of heat loss to the spark plug during the early flame growth by modeling flame initiation and flame propagation around the spark plug. They found that the higher flame travel velocities decreased the heat loss rate and this effect becomes less significant as the flame travel velocities are increased.

1.3 Objectives

Efforts to reduce the exhaust emissions from small utility engines, which contribute a significant proportion to the increase in atmospheric pollution, are presently in introductory states. This study contributes to the ongoing efforts to reduce small engine emissions by evaluating the effect of different ground electrode geometries on exhaust emissions. The objectives of this thesis are:

1. To assess the comparative effectiveness of the Pyrotek spark plugs relative to conventional (Champion) spark plugs by measuring exhaust emissions produced by several small utility engines in controlled experiments.

2. To improve understanding of how and why spark-plug geometry affects the exhaust-gas emissions of such engines.

CHAPTER 2

THEORETICAL / EXPERIMENTAL BACKGROUND ON IGNITION AND FLAME DEVELOPMENT

2.1 Ignition by Spark

Ignition of combustible mixtures can be accomplished by creating a spark by electrical discharge between two electrodes placed in the mixture. The spark is caused either by capacitance discharge (which is relatively fast $\approx 0.01\mu sec$) or by inductance discharge. A capacitance discharge is produced by quickly discharging a condenser, whereas an inductance discharge is produced by opening a circuit, which involves transformers, ignition coils and magnetos.

If C_1 is the capacitance of a condenser, and V_1 and V_2 are the voltages on the condensers respectively before and after the spark, the energy discharged is given by [30]

$$E = \frac{1}{2}C_1\left(V_1^2 - V_2^2\right) \tag{2}$$

The process of ignition of premixed charges is envisaged as occurring in the following manner: the passage of the spark raises the temperature of a small, roughly spherical, volume of air (referred to henceforth as the spark kernel) to sufficiently high value to initiate rapid evaporation of any fuel drops contained within this volume. The subsequent reaction rates and mixing times of air and fuel are assumed infinitesimally fast, so any fuel vapor created within the spark kernel is instantly transformed into combustion products at the (assumed) adiabatic flame temperature. If the rate of heat release by combustion exceeds the rate of heat loss by thermal conduction at the surface of the inflamed volume, then the spark kernel grows in size to fill the entire combustion volume. If, however, the rate of heat release is lower than the rate of heat loss, the temperature within the spark kernel falls steadily until fuel evaporation on the unburned side of the flame front ceases altogether [32].

The size of the spark kernel is of crucial importance, since the rate of heat loss at the kernel surface is just balanced by the rate of heat release, due to the instantaneous combustion of fuel vapor, throughout its volume. This concept leads to the definition of "quenching distance" as the critical diameter that the enflamed volume must attain to propagate unaided. We also define the minimum ignition energy as the amount of energy required from an external source to attain this critical size.

2.2.1 Simplified Ignition Analysis

According to the Williams' second criterion for ignition and quenching, the rate of liberation of heat by chemical reaction inside the volume must approximately balance the rate of heat loss from the volume by thermal conduction. We can apply this criterion to the flame kernel, which represents the incipient propagation flame created by a point spark. We define a critical gas-volume radius such that a flame will not propagate if the actual radius is smaller than the critical value and also assume that the minimum energy supplied by the spark is the energy required to heat the critical volume from its initial state to the flame temperature. To determine the critical radius (R_{crit}), we equate the rate of heat liberated by the reaction rate to the heat lost to the cold gas by conduction, as shown in the Figure 2.

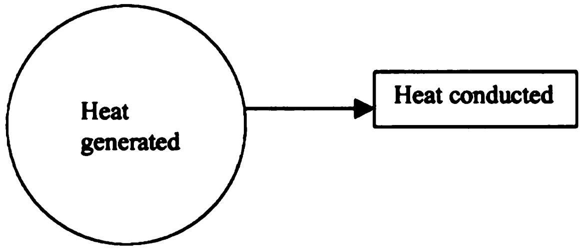

Figure 2: Heat Balance Diagram

$$\dot{Q}'''V = \dot{Q}_{cond} \tag{3}$$

where $Q^{\bullet}{}'''$ is the volumetric heat release rate and

Also

$$\dot{Q}_v''' = -\dot{m}_F'''\Delta h_c \tag{4}$$

$$V = (4/3)\pi R^3. \tag{5}$$

Similarly from the Fourier's law:

$$\dot{Q}_{cond} = -\lambda\left(4\pi R_{crit}^2\right) {dt}/{dr}\big|_{Rcrit}. \tag{6}$$

Here, $m_F^{\bullet}{}'''$ is the mass flow rate (kg/m^3-s) of fuel, and λ is the thermal conductivity of the burned gas. Hence, equation (3) can be written as:

$$-\dot{m}_F'''\Delta h_c(4/3)\pi R_{crit}^3 = -\lambda 4\pi R_{crit}^2\, {dt}/{dr}\big|_{Rcrit}. \tag{7}$$

We have expressed the volume and surface area of the sphere in terms of critical radius in equation (7). The temperature gradient at the gas boundary can be evaluated by determining the temperature distribution of the gas beyond the sphere ($R_{crit} \leq r \leq \infty$) with the boundary conditions: $T_{Rcrit} = T_b$ and $T_\infty = T_u$. This leads to the result

$$dt / dr\big|_{Rcrit} = -\left(\frac{T_b - T_u}{R_{crit}}\right). \tag{8}$$

Substituting (8) in (7) and simplifying we get

$$R_{crit}^2 = \frac{3\lambda(T_b - T_u)}{-\dot{m}_F'''\Delta h_c}. \tag{9}$$

The equation (9) indicates that critical radius strongly depends on the thermo-chemical properties of the mixture.

2.2.1 Laminar Flame Speed

Spark ignition engines with well-designed intake systems are often good examples of an application of premixed combustion. The fuel-air mixture is produced by a carburetor or fuel injection system. Even though the fuel is introduced as a liquid, because it is highly volatile it has time to vaporize and thoroughly mix with the air, before the mixture is ignited by the spark. In some engines, however, the use of short intake systems and close-coupled carburetors inhibits thorough mixing, and combustion may not be completely premixed.

The laminar burning speed is defined as the velocity relative to the flame front, with which unburned gas moves into the front and is transformed to combustion products under laminar flow conditions. The laminar burning velocity (S_l), at pressures and temperatures typical of unburned gas mixtures in engines, is usually measured in spherical closed vessels by propagating a laminar flame radially outward from the vessel center.

According to the Mallard Le-Chatelier flame theory[40], the premixed flame is treated as a travelling wave. The propagation process is viewed as a balance between heat production via chemical reaction and the associated convective and conductive redistribution mechanisms. Consider a flame cross section joining unburned upstream gas and downstream burned gas. In the upstream gas, there must be a balance between downstream convection and upstream diffusion of heat if the flame propagation is steady. Hence

$$\rho C_p S_l (T_b - T_u) = \lambda \frac{(T_b - T_u)}{\delta}$$

or (10)

$$\delta = \frac{\lambda}{\rho C_p S_l} = \frac{\alpha}{S_l} = \frac{\lambda / C_p}{\dot{m}''}. \tag{11}$$

The flame thickness δ is usually of the order of 0.1 cm. The mass burning rate can be given as

$$\dot{m}'' = \rho S_l = W\delta, \tag{12}$$

where *[W] = mass/vol–sec*. In other words, the mass flux into the flame equals the volumetric mass consumption rate W multiplied by the flame thickness δ over which the consumption occurs. Substitution of

$$\delta = \dot{m}''/W \tag{13}$$

gives

$$\dot{m}''^2 = \frac{\lambda}{C_p} W \Rightarrow S_l^2 = \frac{\lambda}{\rho C_p} \bullet \frac{W}{\rho} \tag{14}$$

or

$$S_l = \sqrt{\alpha \bullet RR}, \tag{15}$$

where $\alpha = \lambda / \rho\, C_p$ is the thermal diffusivity and $RR = W/\rho$ is the reaction rate. We can evaluate α in the unburned gas, W at the flame temperature, and ρ (in RR) at the unburned state. We may write

$$RR = \frac{W}{\rho_u} \approx \frac{Y_R^n A e^{-E_a/RT_b}}{\rho_b}.$$

Therefore, S_l can be rewritten as, (16)

$$S_l = \sqrt{\frac{\alpha Y_R^n e^{-E_a/RT_b}}{\rho_u}}.$$

(17)

The laminar flame speed from the above equation indicates a strong dependence on the thermal diffusivity and the reaction rate. The Mallard Le-Chatelier model is useful in estimating the order of the magnitude of flame speeds, but, in reality, the reaction zone is much more complicated than the Mallard Le-Chatelier model indicates.

2.2.1.1 Factors Affecting Flame Speed

2.2.1.1.1 Pressure.

From equation (17), since $\alpha \propto \rho^{-1}$ and $Y_R \propto \rho$,

we obtain $$S_l \propto [\rho^{-1} \cdot \rho^{n-1}]^{1/2} = \rho^{(n/2)-1}. \quad (18)$$

But $\rho \propto P$, so that $$S_l \propto P^{(n/2)-1} \quad (19)$$

By varying the overall pressure, the order of the overall reaction n can be deduced from flame speed measurements.

2.2.1.1.2 Temperature.

From the equation (17), since $RR \propto e^{-E/RT_f}$, this means that $S_l \propto e^{-E/2RT_f}$. Hence the laminar flame speed S_l is extremely sensitive to the flame temperature T_f.

2.2.1.2 Relation between Flame Speed and Critical Radius

Using a series of assumptions [14], and assuming a balance between conduction and convection heat transfer for spherical volume, the critical radius can be related to the laminar flame speed S_l as

$$R_{crit} = \sqrt{6}\,\alpha / S_l \cdot \tag{20}$$

The minimum ignition energy, E_{ign}, can be determined if we assume that the energy added by the spark heats the critical volume to burned gas temperature and can be written as

$$E_{ign} = m_{crit} C_p (T_b - T_u) \cdot \tag{21}$$

Thus

$$E_{ign} = 4\frac{\pi}{3} \rho_b R_{crit}^3 C_p (T_b - T_u) \cdot \tag{22}$$

Substituting (19) into (21), we get

$$E_{ign} = 61.1 P \left(\frac{C_p}{R_b}\right)\left(\frac{T_b - T_u}{T_b}\right)\left(\frac{\alpha}{S_l}\right)^3 \cdot \tag{23}$$

The energy supplied by the ignition systems of SI engines is always greater than the minimum ignition energy required for the successful ignition of the mixture. The initial flame grows under the influence of the following parameters: energy supplied through the spark, heat loss to the electrodes, the effect of strong curvature due to the small radius, and the turbulence in the flow field.

Meghalchi and Keck [31] experimentally determined the laminar flame speeds for various fuel-air mixtures over a range of temperature and pressures typical of conditions associated with reciprocating internal combustion engines. They calculated the burning velocities in a bomb from implied burn rates under the following assumptions:

- The unburned gas is initially at rest and has uniform temperature and composition.
- The thickness of the reaction zone is negligible, and gas within the bomb consists of a burned fraction x at local thermodynamic and chemical equilibrium, and unburned fraction $1-x$ at local thermodynamic equilibrium, but with fixed chemical composition.
- The pressure is independent of position and a function of time only.
- The reaction front is smooth and spherical.

$$S_l = S_{l,0}(T_u/T_0)^{\alpha}(p/p_0)^{\beta}, \tag{24}$$

where

T_0 = 298 k

p_0 = 1 atm

T_u = temperature of the unburned mixture

P = pressure of the unburned mixture

$S_{l,0}$ = constant for a given fuel, equivalence ratio, burned gas dilution fraction

for iso-octanes, these constants can be represented by

$$\alpha = 2.18 - 0.8\,(\phi - 1)\,, \tag{25}$$

$$\beta = -\,0.16 + 0.22(\phi - 1), \tag{26}$$

$$S_{l,o} = B_m + B_\phi(\phi - \phi_m)^2\,, \tag{27}$$

where ϕ_m is the equivalence ratio at which $S_{l,o}$ is maximum with value B_m.

Table 2: Table Of Parameters For Equation 24

Fuel	ϕ_m	*Bm*(cm/sec)	B_ϕ (cm/sec)
Iso-octane	1.13	26.3	-84.7
Gasoline	1.21	30.5	-54.9

2.2.1.3 Heat Loss Effect on the Flame Speed

The effect of heat losses to the electrodes on the laminar flame speed can be modeled in the following way:

$$\Delta S_l = S_{l,adia} - S_{l,nonadia} \tag{28}$$

or

$$Q_{comb} = h_c \, {}^{dm}\!/_{dt} = h_c \rho_u S_l A_f$$

Thus (29)

$$S_{l,adia} = \frac{Q_{comb}}{\rho_u A_f h_c}$$

(30)

The heat transfer from the flame kernel to the electrodes will be convective as well as conductive. Radiation processes are neglected as radiation from flames is mainly due to infrared emissions from CO_2 and H_2O bands [15]. These infrared emissions can not be absorbed by the unburned gas as, CO_2 and H_2O are not available ahead of the flame front [15]. In addition, heat loss can be estimated using the lumped heat transfer coefficient '***h***', and is given by

$$\dot{Q}_{loss} = hA_c(T_b - T_l),$$

(31)

where, A_c is the contact area between the flame and electrodes, T_b is the gas temperature, and T_l is the electrode temperature. The effect of this heat transfer on the laminar flame speed can be written as

$$\Delta S_l = \frac{1}{\rho_u A_f}\left(\frac{Q_{comb} - Q_{loss}}{h_c}\right)$$

(32)

This indicates that with the increase in the heat losses from the flame kernel, the laminar flame speed decreases. This reduction in the laminar flame speed strongly depends on the contact area fraction f_c, defined as the ratio of the contact area A_c to flame surface area A_f. (a sphere of radius r_f).

$$f_c = \frac{A_c}{A_f} = \frac{Ac}{4\pi r_f^{\,2}}. \tag{33}$$

This heat loss from the flame kernel affects the flame kernel growth through two mechanisms:

- It decreases the kernel temperature leading to a relative contraction of the kernel, due to its lower density.
- It transfers heat from the flame front, thereby decreasing the burning velocity.

In order to have a significant impact on the flame growth, the heat loss from the initial flame kernel has to be comparable to the energy gain rate from combustion. This ratio can be estimated by using a laminar burning speed S_l.

$$\frac{\dot{Q}_{loss}}{\dot{Q}_{comb}} = \frac{hA_c(T_b - T_l)}{\rho_u A_f S_l h_c}. \tag{34}$$

The ratio in equation (34) has to be greater than one, in order to have a successful flame initiation.

2.2.1.4 Flame Stretch Effect

The effects of flame stretch are to reduce the area available for flame propagation and also to increase the heat losses from the stretch surface of the unburned mixture [29]. The strong curvature of a spherical flame kernel may also considerably slow the flame speed. Markstein [30] suggested a linear dependence of laminar flame speed on flame stretch given by:

$$S_{l,s} = S_{l,adi} - M_a \delta K, \tag{35}$$

where:

Ma is the Markstein number

$S_{l,s}$ is the adiabatic stretched laminar flame speed

K is the stretch factor and

$K = (2/r_f)(dr_f/dt)$, for a spherical flame propagation, (r_f) being the flame kernel radius. This equation indicates that larger initial flame kernels will have smaller stretch factors, and therefore, a lower reduction in laminar flame speeds.

2.2.2 Turbulent Flame Speed.

Whereas the laminar flame speed has a propagation velocity that depends uniquely on the thermal and chemical properties of the mixture, a turbulent flame has a propagation velocity that depends on the characteristics of the flow, as well as the mixture properties. A simple theoretical formula proposed by Damkohler for the turbulent flame speed is given by

$$S_t = S_l + u', \tag{36}$$

where u' is the scale of turbulent velocity fluctuations (m/s).

The flame is assumed to spread by the process of turbulent entertainment, with burning occurring in the entrained region at a rate controlled by the turbulent parameters. The flame front is assumed to entrain mixture at a rate that is governed by the turbulent intensity and the local laminar flame speed. Thus, the burning rate can be given by

$$\frac{dm}{dt} = \rho_u A_f (u' + S_l) \tag{37}$$

where:

m = mass entrained in to the flame front

ρ_u = density of the unburned charge

A_f= flame front area (excluding area in contact with the electrode surface)

u'=turbulent velocity factor

Turbulence is typically inhomogeneous and always time varying. Chen and Veshagh [17] assumed the following to express turbulent intensity:

- The turbulent flow is isotropic and homogeneous over the combustion period near the compression.
- The turbulence velocity factor is proportional to the mean piston speed and does not change substantially over the combustion period:

$$u' = cV_p \tag{38}$$

where V_p is the mean piston speed and c is the constant, which depends on the design of the inlet port, the inlet valve shape, and many other factors.

- The integral length scale (l_0) retains a constant value over the combustion period. This assumption is roughly correct, as some studies suggested that the integral scale almost maintains a constant value over the compression TDC position [16].

Semenov [36] suggested the following expression for turbulence intensity, as governed by the conservation of angular momentum:

$$u' = u'_{ig}\left(\frac{\rho_u}{\rho_{u,ig}}\right)^{1/3} \tag{39}$$

Here, the subscript ig is for the values at the time of ignition and subscript u is for the values of unburned mass. Although many different theoretical formulae have been developed to predict the turbulent flame speed, there appears to be general agreement that turbulent flame speed depends only on turbulent intensity and does not involve any other turbulence property, such as the such as length scales, etc.

2.3 Burn Duration

The rate at which fuel-air mixtures burn increases from a low value, immediately following the spark discharge, to a maximum, about half way through the burning process. This burning rate then decreases almost to zero as the combustion process ends. It is convenient to use mass-fraction burned to characterize different stages of the spark ignition engine combustion process by their duration in crank-angle degrees, thereby defining the fraction of the engine cycle that they occupy. The flame development process from spark discharge, which initiates the combustion process to the point where a small but a measurable fraction of the charge has burned, is one stage. It is influenced primarily by the mixture state, composition, and the motion in the vicinity of the spark gap. The major portion of the charge burns as the flame propagates to the chamber wall, in the second stage. This stage is obviously influenced by thermodynamic conditions throughout the combustion chamber. The final stage, when the remainder of the charge burns to completion, can not be quantified easily because energy release rates are comparable to other energy transfer processes that are occurring.

A functional form often used to represent the mass fraction burned versus the crank angle curve is the Weibe function.

$$x_b = 1 - \exp\left[-a\left(\frac{\theta-\theta_0}{\Delta\theta}\right)^{m+1}\right] \tag{40}$$

Here, θ is the crank angle, θ_0 is the start of combustion, $\Delta\theta$ is the total combustion duration ($X_b = 0$ to $X_b = 1$), and a and m are adjustable parameters. Varying a and m changes the shape of the curve significantly, actual mass-fraction-burned curves have been fitted with a =5 and m=2. The crank angles can be converted to time (in seconds) by dividing by 6N (with N in rev per min).

It has been observed experimentally [24] that during cycles in which the flame kernel moved towards the center of the combustion chamber, the burn duration was shorter than during cycles in which it moved away from the center of the cylinder. The factors affecting the burn duration are given at Appendix A.

2.3 Effect of Initial Flame Kernel Growth

The initial flame kernel growth has a strong influence on the overall combustion process in the IC engines. The parameters governing the initial flame kernel growth and subsequent flame propagation are:

- The ignition system, which includes the spark duration and ignition energy.
- Effect of electrical energy on flame growth.
- Heat losses to the electrodes.
- Flame kernel advection from the spark gap.
- Characteristics of charge motion.
- Effect of convection velocity.

The details of these parameters are discussed in Appendix B.

CHAPTER 3

EXPERIMENTAL APPARATUS AND PROCEDURES

3.1 Experimental Set Up

In order to evaluate the comparative effectiveness of the Pyrotek spark plug and a base-line Champion spark plug, emission measurements were carried out for three different types of test engines. The details of these test engines are listed in Appendix C. The emission measurements of these engines were carried out in the sequence described below.

The two stroke Homelite Super 2 chainsaw engine was mounted on a Homelite eddy current dynamometer in a test cell. The ambient temperature in the test cell was held within a few degrees of constant value and was always between a 20°C to 30°C limit. The four stroke Tecumseh VLV60 side valve engine and Tecumseh OHH50 overhead valve engines were mounted on a Micro-Dyn 15 hydraulic dynamometer, in the same test cell as the chain saw engine. The four stroke engines were mounted on a hydraulic dynamometer and could be run at a constant programmed speed, while the torque output produced by the engines was measured.

Each engine was run according to the appropriate EPA CFR test procedure, using Indolene (or Indolene mixed 32:1 with two-stroke oil for two-stroke engine). This fuel was supplied to the engine by a fuel cart, which measured the mass flow rate of fuel consumed by the engine. On this cart, a Micro Motion Coriolis meter DS0006S100 carried out the fuel flow measurement. Fuel was supplied to each engine at a constant pressure with the level of fuel at the height of the half-full level of the original fuel tank of each engine. The engine exhaust gases were ducted though a dilution tunnel positioned in a manner such that all the exhaust products and sufficient quantities of ambient dilution air were drawn through it.

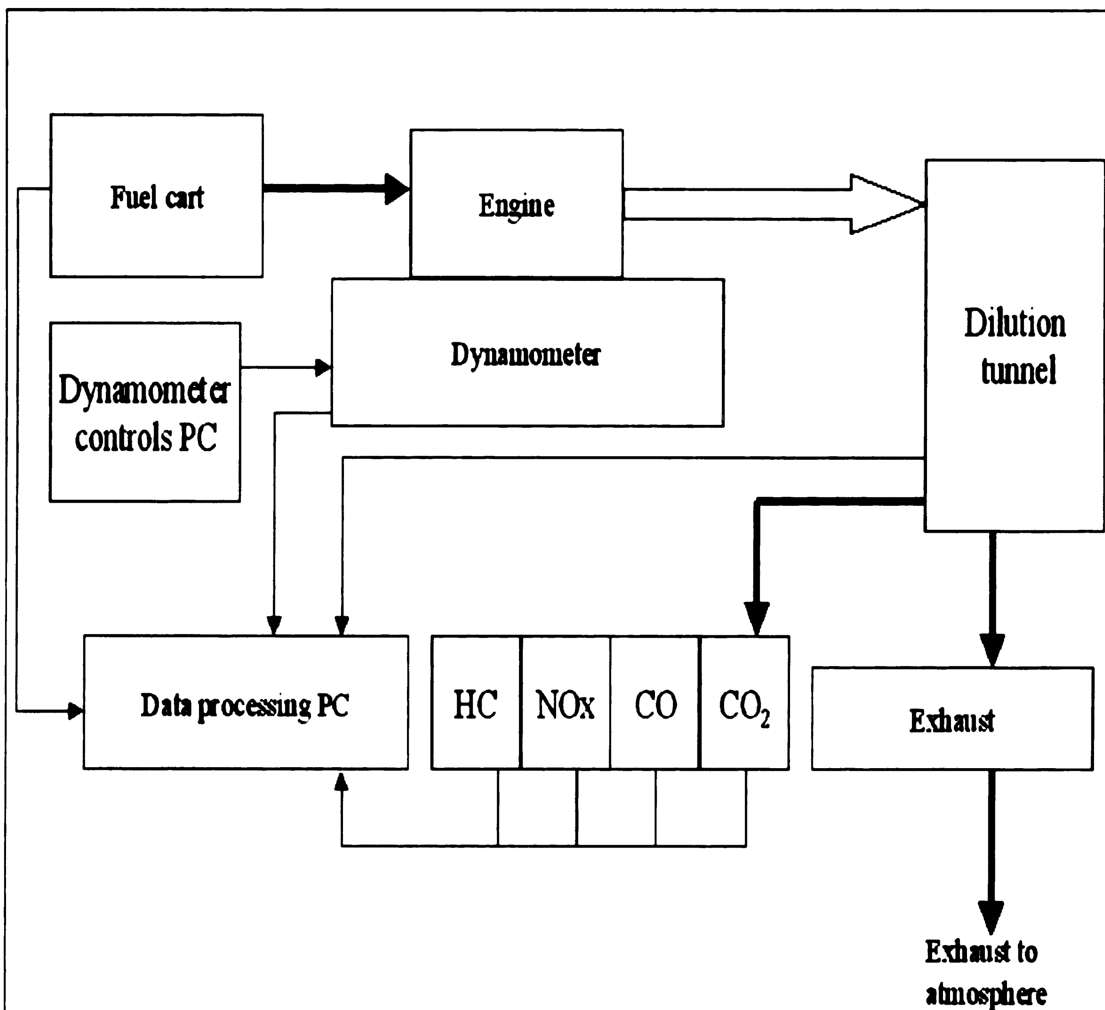

Figure 3: Layout of Test Equipment

The intake of the dilution tunnel was positioned slightly away from the muffler to avoid any chances of creating unnecessary vacuum or additional suction on the muffler. This diluted mixture of exhaust gases was then drawn through a critical flow nozzle by a ring compressor. The critical flow nozzle regulates the total flow rate of ambient air and exhaust gases. The size of the critical flow nozzle was changed between the tests in order to make best use of the measurement range of the emission analyzer. A partial sample of this diluted mixture was fed to the emission analyzers, while remaining gases were expelled from the test cell. In addition, during periods of exhaust-gas sampling, the background level of ambient air were also recorded and subtracted from the final data output.

Diluted exhaust-gas samples were analyzed continuously throughout each test for their CO, CO_2, HC (propane equivalent), and NO_x content by a Horiba Model 11136-1 emission bench. The details of the layout are given in Figure 3. A brief overview of the working principles of the Horiba emissions bench is given at Appendix D and more complete details are given in [23].

3.1.1 Test Equipment Calibration

The emission analyzers were calibrated before the start of tests using a gas divider at 10, 20, 30, 40, 50, 60, 70, 80, and 90% settings between the span and zero concentrations. While the CO_2, HC and NO_x responses were linear to better than the required 2% accuracy throughout their range, the response of the CO analyzer was fitted with a fourth- order polynomial to achieve better than 2% accuracy.

The torque calibration on the dynamometer was performed by adding different weights at a distance of 45.72cm (18 inch) from the torque-sensor load cell. All indicated torques were within 2% of the applied torque.

By checking the fuel flow through the Micro Motion meter for specified time, and collecting and weighing the fuel in the beaker, the calibration of the fuel flow meter was verified to better than 1% accuracy. The fuel filters of the fuel cart were regularly renewed. Vibrations in the fuel cart attributed to the fuel pumps were minimized by mounting the pumps externally. Additional filters were also installed to further damp vibrations which would otherwise cause inaccurate meter readings.

3.1.2 Recorded Data

In addition to the emission data, a number of other quantities were also measured along with the exhaust emissions. These included engine speed (RPM), torque output, power output, the atmospheric and differential pressure, cylinder head temperature, room and exhaust temperatures, relative humidity, and fuel flow rates.

3.2 Test Procedure

The test procedure detailed in the CFR40 part 90 was followed where applicable. All the equipment was calibrated prior the commencement of tests. For the gas sampling test procedure, analyzers were turned on for a period of half an hour to give it a sufficient time to warm up. Next the analyzers were zeroed, spanned, and tested for the HC hang up, before all the tests. Background concentrations of the ambient air (dilution air) during the each test were also taken in order to include the background effect. Every effort was made to complete each particular test in the same day in order to reduce the variations of the test parameters due to the changes in the ambient conditions. The test engines were warmed up until the exhaust temperature stabilized at a particular throttle setting or load. This was done to ensure the same conditions for each test. Before the commencement of each test, the spark gap of the spark plugs was adjusted to the engine manufacturer recommendations. A sample data sheet indicating measured and calculated quantities is given in Figure 4 below.

```
Emissions                        Operating Conditions         Temperatures
---------                        -------------------          ------------
 Fuel flow  (gr/hr) 423.7        Speed (rpm)       2797.
 HC (C_1)  (    ) .1802          Power  (brake hp) 1.3883      T_nozzle (`C)    46.9
 NOX       (    ) .3232          Torque    (ft-lb) 2.606       T_cyl   (`C)   103.0
 CO2       (    ) .5228          Rel. Humidity (%) 15.00       T_exhaust (`C)  253.8
 CO        (    ) .3594          T_room    (`C)    30.5        T_oil    (`C)   27.6
 CH4       (    ) .0000          P_diff   (kPa)   .110         T_fuel   (`C)   27.3
                                 P_abs    (kPa)   97.5

CO(g/kW/hr); NOx(g/kW/hr); HC(g/kW/hr); CO2(g/kW/hr)
CO(g/hp/hr); NOx(g/hp/hr); HC(g/hp/hr); CO2(g/hp/hr)

    54.7      8.0      4.88    1147.10
    40.8      5.9      3.64     855.74

  CO(grm/hr);  NOx(grm/hr);  HC(grm/hr);  CO2(grm/hr)

    56.7      8.2      5.05    1188.02
BSFC (gr/kW/hr) :  409.08  Fuel burned (%) :   98.81
Dil. Fac   30.66 Dil. Fac (EPA)  29.73 AFR  :    13.94
[CO]/[CO2]   .0477
```

Figure 4: Output Data File Indicating Measured and Calculated Quantities

3.2.1 Air-Fuel Ratio

The air fuel ratio was calculated according to Spindt's method- an equilibrium combustion model equation involving fuel composition and exhaust gas composition only. For this method, exhaust gas concentration was determined using the emission analyzer. Following ratios were calculated using the concentration of the CO, CO_2, O_2 and hydrocarbons (per carbon atom) and known fraction of carbon in the fuel (F_C):

$$R = P_{CO} / P_{CO_2}, \tag{41}$$

$$Q = P_{O_2} / P_{CO_2}, \tag{42}$$

$$F_b = \left(P_{CO} + P_{CO_2}\right) / \left(P_{CO} + P_{CO_2} + P_{CH}\right). \tag{43}$$

Then,

$$A/F = F_b\left[11.492 F_C\left(\frac{1 + R/2 + Q}{1 + R}\right) + \frac{120(1 + F_C)}{3.5 + R}\right]. \tag{44}$$

The accuracy of this method when compared with measured air-fuel ratios was found to be above 95% even for poor combustion. The comparative results along with detailed calculation are given in [37].

3.2.2 Two Stroke Chainsaw Engine

The two stroke Homelite Super 2 chainsaw engine was controlled manually by its throttle cable. The emission measurements were made at two settings: idle and wide open throttle. The engine was locked at wide-open throttle to test it at rated mode, and locked at the closed (idle) position for the idle mode. In this case, the idle mode was quite variable from test to test, possibly because of the length of the time required to reach a steady state. The CFR requirement of steady state, in which the cylinder head temperature remains within a 10°C band for three minutes, was met in all tests.

A series of idle tests was carried out in which the engine was run with one spark plug, until a nominally steady state was reached and data was then taken. Then another idle test was performed with a different spark plug, and so on. It was found that the sequential tests at one mode were more repeatable. Therefore, all three spark plugs were first tested at idle.

Some minor adjustments had to be made to the engine carburetor in order to find an idle mixture/speed at which the engine would run evenly for all three spark plugs tested. At wide-open throttle (WOT), no such difficulty was encountered.

3.2.2 Four Stroke Utility Engines

Two different types of four stroke engines were used as described in sect 2.1. These four stroke utility engines were mounted on the hydraulic dynamometer cart. In order to control the engine speed and throttle settings more precisely, the engine governor was disconnected and an external throttle cable was connected instead. The use of the external throttle cable provided much more stable engine performance than did the engine governor. Before taking the emission data, each engine was run at its maximum rated load (maximum power output) at 2800 rpm, and its torque was recorded. Once the WOT power was known, these engines were run at various fractional loads (100%, 75%, 50%, 25%, 10% of the WOT power achieved) as required by CFR40 part 90. Two different approaches were adopted for each engine when run at various fractional loads. In the first approach, the engine was run at all five load settings in sequence with the same spark plug, prior to changing to a second plug. In this approach, the load settings at which the engines operated could not be repeated precisely, and, consequently, they operated at slightly different air to fuel ratios. In the second approach, at each setting, the engine was operated at a given load with each of the spark plugs installed, with no changes made to the throttle, speed and load setting. The data collected in this approach was found to be more consistent since, at a given load, the engine operating at essentially the same air to fuel ratio.

The engines were also run at the idle settings by disconnecting the engine from the dynamometer. The carburetors of the four stroke utility engine were of fixed jet design, with no adjustment available. In the idle mode (about 1500 rpm), all three spark plugs chronically misfired occasionally, although no chronic misfires were observed in any of the other load settings. The repeatability of tests of the four stroke engines was higher than the two-stroke engine, with the highest repeatability being for the Tecumseh overhead valve engine. The entire tests were repeatable within five percent of any brake specific emissions measurement.

Apart from the effect of each spark plug's different ground electrode geometry on engine emissions, other aspects of spark plugs on engine emissions were also analyzed. These included the spark plug orientation, spark gap, center electrode geometry, and engine speed.

CHAPTER 4

TEST RESULTS

4.1 Overview

A comparison between the emissions/performance of three different engines fitted with: i) a brand-new spark plug of the manufacturer's recommended Champion model (the baseline plug); ii) a brand-new Pyrotek (crown-shaped electrode) version of the baseline plug; and iii) a well-used Champion spark plug was carried out. Effects of different ground electrode geometries would then be revealed by differences between the Pyrotek (new) and the baseline (new) spark plugs. Changes in performance through usage could also be assessed by carrying out the same tests with a well-used Champion sparkplug, which would be indicative of emissions levels during normal usage of these engines. The two stroke Homelite Super 2 chainsaw engine (1 hp) engine was tested with all three kinds of spark plug (baseline Champion model DJ7Y). The four stroke sidevalve (L-head) (Tecumseh VLV60, Champion J19LM) and overhead valve (Tecumseh OHH50, Champion N4C) engines were tested principally with the Pyrotek (new) and baseline (new) spark plugs, to clearly differentiate the effect of ground electrode geometry. The results are discussed in the order in which these tests were performed. Details of these results in tabulated data form are presented at Appendix E.

4.2 Two Stroke Homelite Super 2 Chainsaw Engine

Two stroke Homelite Super 2 chainsaw engine used in this study was a well used engine with over 50 hours of operation. For this engine, the tests performed were basic CFR40 comparisons of the emissions levels of this engine with three different types of spark plugs, i.e. Pyrotek, a brand new Champion spark plug and a well used Champion spark plug. In these tests, the engine was operated at first at wide-open throttle and then at idle. Each test was then repeated so that three-test averages could be constructed. Figure 5 shows the comparative level of hydrocarbon emissions for the three spark plugs at these two throttle positions.

At 6% load (the nominal idle), the difference between emission levels was not very distinct. However, at WOT, the difference in the emission level was quite significant. There was approximately a 13% reduction in the hydrocarbon emissions when using the Pyrotek spark plug compared to the brand new spark plug. In addition, a 17% reduction in hydrocarbon emissions was observed when compared with the well used spark plug. The results in Figure 7 show that NO_x emissions were higher for the pyrotek spark plug as compared to the new and well used Champion spark plugs. Although the NO_x emissions were quite low in total, relative to regulatory standards for small engines, the trend indicates that the Pyrotek plug produces more NO_x with a subsequent reduction in the hydrocarbon emissions. Moreover, at the same throttle setting the Pyrotek produces 4.5% and 12% more torque than the new spark plug and the well used spark plugs respectively as shown in Figure 6.

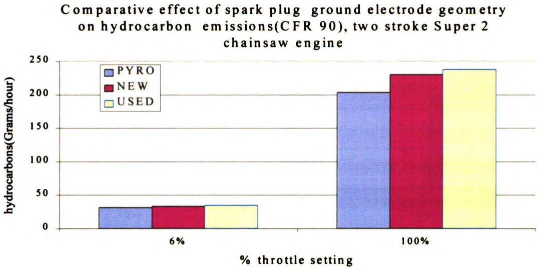

Figure 5: *HC* vs % Throttle Setting for Three Spark Plugs

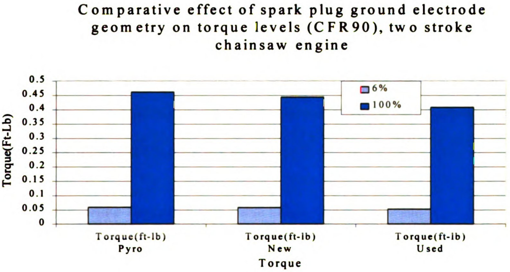

Figure 6: Torque vs Three Spark Plugs

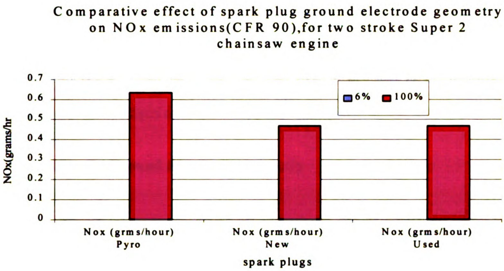

Figure 7: NO_x vs Three Spark Plugs

After three successive tests with a given spark plug at a given mode, the only change made was to replace one spark plug with another, restart the engine, and run it until it had fully warmed up. Comparisons of results from successive tests with the same spark plug indicated the repeatability of the emissions measured was about 5% for this two-stroke engine. Since the reduction in emission achieved with the Pyrotek plug was considerably more than this uncertainty, it was considered a significant effect attributed to geometric differences in the spark plugs.

4.3 Four stroke Tecumseh side valve (VLV60) utility engine

The side-valve engine used in these studies was a brand new engine which had been broken in for six hours in accordance with the manufacturer's recommendations. The engine was run at WOT, the maximum torque at its rated speed of 2800 rpm was recorded, and the engine emissions were then measured according to CFR90 procedures.

In studies of the Tecumseh side valve engine operating with different spark plugs, emissions were measured at each of 6 loads required for a CFR40 certification test, as well as comparing emissions as functions of angular position of the spark-plug ground electrode and as functions of different spark-plug gaps.

4.3.1 Effect Of Ground Electrode Geometry

In this test, the effect of ground electrode geometry on emissions was evaluated. The procedure adopted was to record the maximum torque produced at WOT and then to measure emissions according to CFR90 requirements. These requirements specify that the engine be operated at full (100%) load and subsequently at 75%, 50%, 25%, and 10% of its full load, as well as at idle. These tests were repeated three times for each spark plug. The procedure of adjusting the throttle to achieve target loads, for each of three different spark plugs, resulted in the engine operating at slightly different air-to-fuel ratios for each plug, at nominally the same load. This added variability in air-fuel ratio was believed to obscure the effect of ground electrode geometry on emissions measurements.

Figure 8 shows the hydrocarbon emission levels for the Pyrotek and baseline spark plugs for this side valve engine. It can be seen that there was a significant reduction in hydrocarbon emissions in the case of Pyrotek spark plug, at 50% and 75% load. However, at these loads, the engine fitted with the Pyrotek plug operated at an air-to-fuel ratio slightly higher than it did when fitted with the baseline spark plug as can be seen from Figure 9. A similar trend is observed for the NOx emissions shown in Figure 10.

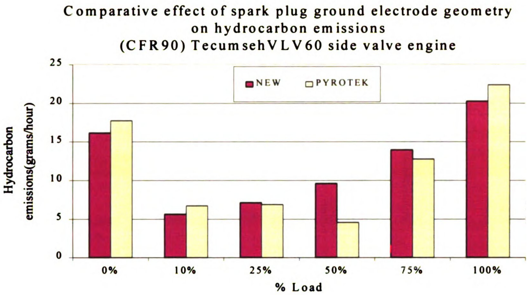

Figure 8: HC Emissions vs % Load

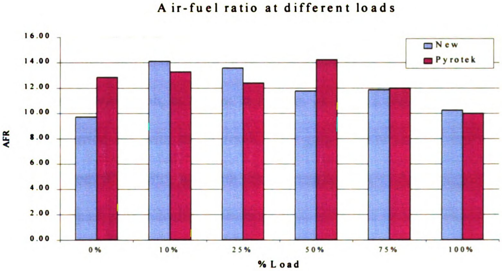

Figure 9: AFR vs % Load

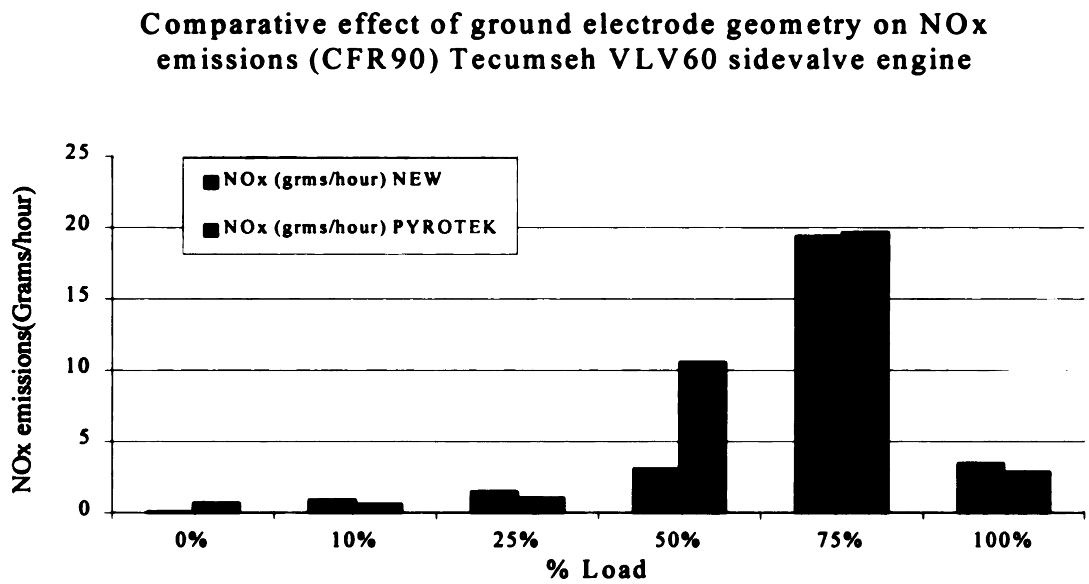

Figure 10: *NOx* vs % Load

4.3.2 Effect of Ground Electrode Orientation

In this series of tests, emissions of the side valve engine were measured when the ground electrode was oriented in each of several different angular positions. The ground electrode oriented with its open end facing the exhaust valve was taken as the datum, and regarded as 0° orientation, as shown in Figures 11 and 12. Successive emissions tests were then carried out with the Pyrotek spark plug rotated counter clockwise at 45° increments from 0° to 180°, and with the baseline Champion spark plug rotated at 90° increments. Spark plug indexing washers of thickness 0.030-inch, 0.004-inch, 0.005-inch and 0.060-inch were used to permit the required orientation to the spark plugs without damaging the cylinder threads. The change in spark plug position had negligible effect on compression ratio as illustrated by calculations in Appendix F. These effects of angular position on emissions were monitored at two load settings: first, at the idle condition with the engine disconnected from the dynamometer; and second at 38% of full load. The emissions measured with the Pyrotek spark plug revealed there was a significant influence of ground electrode orientation on the combustion characteristics.

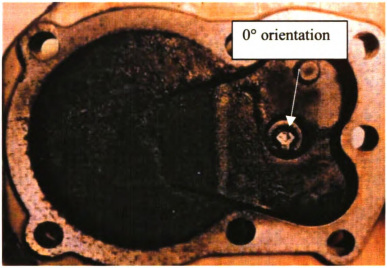

Figure 11: spark plug 0° orientation

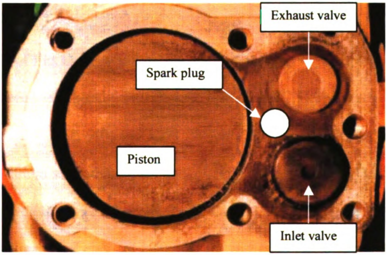

Figure 12: Layout of Combustion Chamber

In comparison with the baseline spark plug, changes in emissions (particularly hydrocarbon emissions) through rotation of the Pyrotek spark plug were large. Five angular positions at part load and two at no-load settings were considered. In the case of the baseline spark plug, only three angular positions were studied at part load. These changes in the hydrocarbon emissions for different orientation angles are shown in Figure 13.

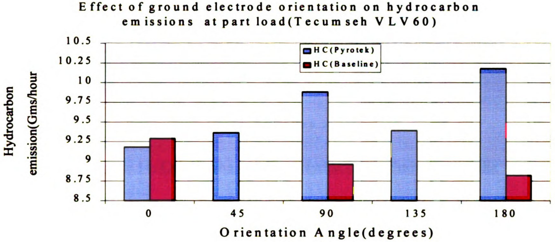

Figure 13: Orientation Angle vs *HC* Emissions at Part Load

The results of Fig.13 show that the Pyrotek spark plug was more sensitive to the orientation compared to the baseline spark plug, with improved emission performance at orientation angles of 0°, 45°, 90°, and 135°. Of these positions, the 0° orientation gave the lowest hydrocarbon emissions. The performance of the Pyrotek spark plug when facing the inlet valve (180°) was inferior to the 0° orientation. Changes in hydrocarbon emissions for base line spark plug are quite low when compared to the estimated test-to-test uncertainty level of 3%. Thus, it is possible that there may not be any real change in hydrocarbon emissions for different orientations of the baseline spark plug.

At idle, with the Pyrotek ground electrode facing the center of the cylinder (90°orientation), the unburned hydrocarbons were significantly (50%) lower than when facing the nearest wall (270°orientation).

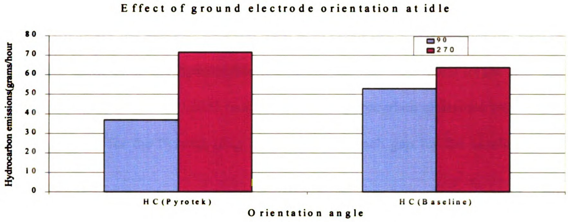

Figure 14: Orientation Angle vs Hydrocarbon Emissions at Idle

No significant effect on hydrocarbon emissions was observed when the baseline spark-plug electrode was rotated, as is evident from Figures 13 and 14. The results were almost identical for all three orientations at part load. In case of the idle tests, the hydrocarbon emissions with the ground electrode facing the center and the nearest part of the cylinder wall were scarcely different.

4.3.3 Influence Of Spark-Plug Gap

In this series of experiments, the gaps of the Pyrotek and baseline spark plugs were varied from .0025 inch to 0.0045 inch, and the corresponding effects on emissions measured. These tests were performed at a fixed throttle setting corresponding to no load, with using spark plugs with the different gaps in successive tests. The changes observed in the hydrocarbon emissions when changing spark gaps are shown in Figure 15. It was observed that *HC* emissions measured with the Pyrotek spark plug were more sensitive to the spark gap used than when the baseline spark plug was fitted. There was a 13% increase in the *HC* emission level when the spark gap was reduced from the recommended 0.0030 inch to 0.0025 inch. In addition, the hydrocarbon emission level increased whenever the gap was changed from 0.003 inch to a larger gap. In the case of the baseline spark plug, the hydrocarbon emissions did not vary much as the gap was changed from 0.0025 inch to 0.0035 inch. The lowest hydrocarbon emissions were found at a gap of 0.003 for the Pyrotek plug and at a 0.0035-inch gap for the baseline spark plug.

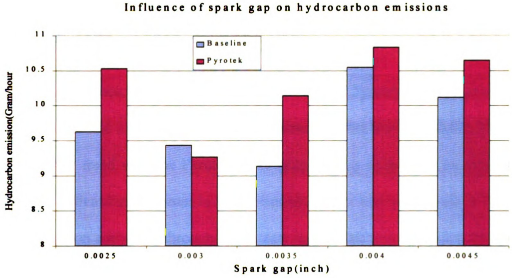

Figure 15: Spark Gap vs HC Emissions

4.4 Four stroke Tecumseh overhead valve (OHH50) utility engine

The overhead-valve engine used in these studies was a brand new engine which had been broken in for four hours according to the manufacturer's recommendations. The engine was run at WOT, the maximum torque at its rated speed of 2800 rpm was recorded, and the engine emissions were then measured according to CFR90 procedures. Emissions tests were carried out at 100%, 75%, 50%, 25%, and 10% of the maximum load and at idle. In these experiments, at each throttle setting, the three spark plugs were tested in succession. In this way, all comparative tests at the same load were performed at identical throttle settings and at about the same air fuel ratios, making it easier to identify the effect of using a particular spark plug. In addition to the 6-mode CFR90 emissions tests on conventional and crown-shaped (Pyrotek) plugs, a series of experiments was performed to examine some effects on engine emissions of center electrode geometry, and engine speed at part load. The details of the tests carried out are discussed separately in the following sections.

4.4.1 Effect Of Ground Electrode Geometry

The hydrocarbon emissions for the baseline and Pyrotek spark plugs are shown in Figure 16 and the corresponding NO_x emissions are displayed in Figure 17. The data show a clear trend with the Pyrotek spark plug tending to produce lower hydrocarbon emissions with a slight increase in NO_x emissions. There was, on average, a 7% reduction in hydrocarbon emissions throughout the test range. This reduction in hydrocarbon was most pronounced at 100% load and least significant at 75% load. There was no significant change in hydrocarbon emissions on account of using different spark plugs at idle. In the case of NO_x emissions, this trend is almost reversed. Increases in the NO_x emissions were significantly lower than decreases in hydrocarbon emissions when substituting a Pyrotek for a baseline spark plug.

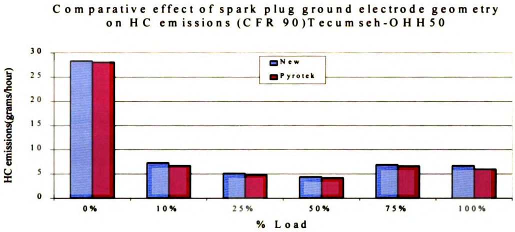

Figure 16: HC vs % Load

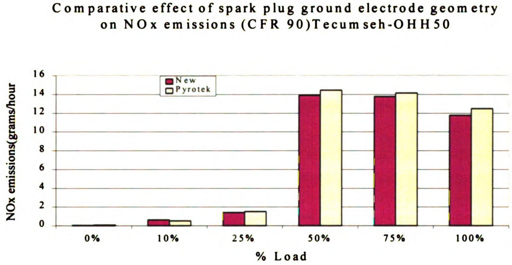

Figure 17: NO_x Emissions vs % Load

4.4.2 Effect Of Center Electrode Geometry

The spark discharge from the Pyrotek spark plug was studied in its original cylindrical shape and when modified by inserting a V-notch in the center electrode. It was observed that, in the case of the unmodified Pyrotek plug, the spark travels from center electrode edges to the ground electrode along the shortest path. Multiple exposure photographs of the spark discharge in quiescent ambient air were taken and the paths followed by sparks for both spark plugs are shown in Figure 18.

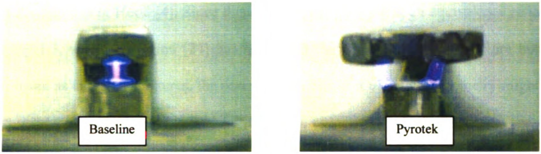

Figure 18: Spark Patterns For Two Spark Plugs

Figure 18 indicates that, in the case of the Pyrotek plug, sparks were only observed at the outer edges of the center electrode. This observation suggested that the middle of the center electrode's upper surface does not participate in the discharge process, and so it might serve only to conduct energy away from the initial flame kernel. Hence, it was decided to make a V-notch in the pyrotek spark plug in order to reduce the contact area fraction of the electrodes and possibly reduce heat losses.

A V-notch was made in the center electrode and another series of tests comparing the engine emissions using these three types of spark plugs was carried out. Figure 19 shows the spark pattern observed with the Pyrotek plug with its center electrode geometry modified in this way. The spark discharge patterns in Figures 18 and 19 appear to be qualitatively the same so this modification may have remedied some disadvantage of an unnecessarily large contact area ratio. Figures 20 and 21 shows the emission levels for the three types of spark plugs installed in this overhead-valve engine. When using the V-notched center electrode, a 6.5% reduction in the hydrocarbon emissions was observed relative to the unmodified Pyrotek spark plug and an 11% reduction was achieved compared to the baseline spark plug. The V-notch geometry was found to be particularly effective in reducing hydrocarbon emissions at low loads. This observation is consistent with the findings of Hood [4]. Since this engine was operating at an equivalence ratio of roughly 1.3, where Heywood [24] has noted that these heat transfer effects are not as significant as at leaner mixtures, the potential benefits of the V-notch geometry might be even greater at equivalence ratios closer to 1. The reduction of electrode contact area by making a V-notch indicates that the heat loss from the flame kernel to the electrode plays an important role in the flame propagation characteristics of spark ignited flames.

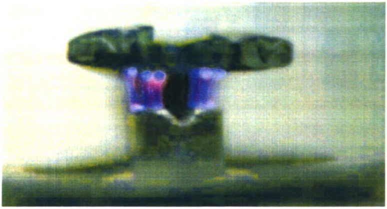

Figure 19: Pyrotek Spark Plug Center Electrode Geometry (V-notch) and Spark Pattern

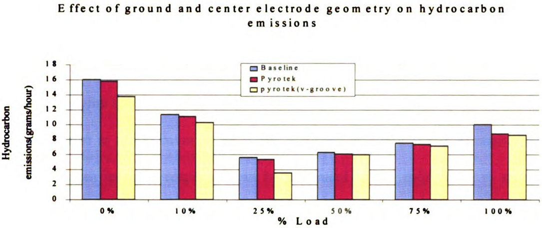

Figure 20: *HC* Emissions vs % Load

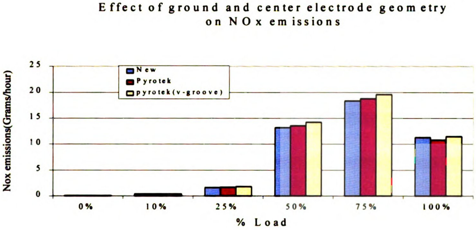

Figure 21: NO_x Emissions vs % Load

4.4.3 Effect of Engine Speed On Engine Emissions

A series of experiments were carried out at fixed throttle settings and different engine speeds to explore how ground-electrode geometry might affect engine emissions at different engine speeds. In these tests, all other controllable parameters were kept constant while the engine speed was changed from 2400 rpm to 3000 rpm. The changes in specific and brake-specific hydrocarbon emissions as functions of engine rpm are shown in Figure 22 when using baseline and unmodified Pyrotek spark plugs. When fitted with the Pyrotek spark plug, hydrocarbon emissions decreased almost linearly with increasing engine speed. In contrast, emissions of this engine equipped with the baseline spark plug rise to a maximum at 2600 rpm and then decrease at higher engine speeds. The differences in these responses can be attributed to the differences in spark-plug geometry. A possible interpretation is that each electrode may influence bulk gas motions in the vicinity of the spark-plug gap differently, which is consistent with the findings of Halldin [38].

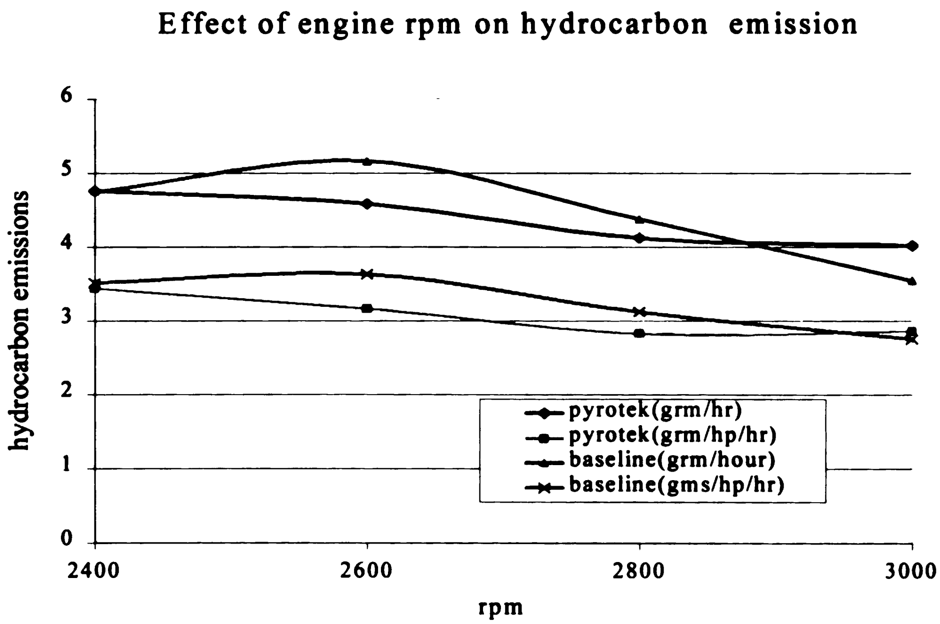

Figure 22: Hydrocarbon Emissions vs Engine RPM

CHAPTER 5

DISCUSSION OF RESULTS

5.1 Effect of Ground Electrode Geometry

The use of the Pyrotek spark plug has been shown to consistently reduce hydrocarbon emissions at the expense of increasing NOx emissions, for a two stroke chainsaw engine (nominally operating at $\phi \cong 1.5$) and for two four stroke utility engines ($\phi \cong 1.3$, side valve & $\phi \cong 1.35$ overhead valve). This reduction in hydrocarbon emissions, and increase in NO_x and torque is consistent with a faster burning rate, which would reduce the burn duration and would cause lower hydrocarbon emissions. A possible explanation for this reduction in hydrocarbon emissions and increase in NO_x emissions is that the Pyrotek ground electrode geometry favors a larger initial flame kernel. As was shown in Figure 18, in section 4.4.2, the electrical discharge in the pyrotek plug is over a longer path than in the baseline spark plug, which therefore leads to a larger initial flame kernel. It is known that larger initial flame kernels increase the burning rates, torque, and NOx emissions and lower the hydrocarbon emissions [20]. Maly [20] experimentally compared the influence of the breakdown, arc, and glow phases of the discharge on engine performances and noted these effects. In these experiments, he noticed that flame kernels with the largest radii, in the breakdown phase, caused the highest NO_x levels whereas flame kernels of the smallest radii (achieved with Capacitor Discharge Ignition

(CDI) resulted in the lowest NO_x concentrations, with corresponding reductions in hydrocarbon emissions at near stoichiometric mixture compositions.

Larger initial flame kernels increase the burning velocity and reduce the burn duration, when other parameters, including the air fuel ratios, are unchanged. They are discussed in detail below. The burn rate is given by

$$\frac{dm_b}{dt} = \rho_u A_f S_l \tag{45}$$

and for a fixed laminar flame speed, greater flame area correspond to faster burn rates. If the Mallard-Le-Chatalier model is applied to the flame front spread in an IC engine, and the flame kernel is initially at its adiabatic flame temperature:

$$S_l = \sqrt{\alpha * RR} \cdot \tag{46}$$

substituting (46) into (45), we get

$$\frac{dm_b}{dt} = \rho_u A_f \sqrt{\alpha * RR} = \rho_u (4\pi r_f^2) \sqrt{\alpha * RR}. \tag{47}$$

Then a larger initial flame kernel radius equates to a faster burn rate. Higher burn rates reduce the burn duration, reduce the total heat losses through time dependent heat transfer and so result in maintaining higher burned gas temperatures, and according to the Mallard Le-Chatalier flame theory, higher reaction rates/ flame speeds.

Another possible explaination is that convection velocities in the vicinity of the spark gap, which would convect the flame kernel away from the electrodes, are enhanced by the crown shape of the ground electrode. They would then increase the flame kernel growth rate by reducing heat losses to the electrode [24]. Heywood [24] using Schlieren photography, observed that the flame kernels which move away from the electrodes grow faster. If the ground electrode of the Pyrotek spark plug (Figure 23) also changed the turbulence intensity in the vicinity of the electrodes, it might also promote a faster initial flame kernel development than with the baseline spark plug. According to the Brown, Stone and Beckwith turbulent combustion model [41]:

$$\frac{dm}{dt} = \rho_u A_f (u' + S_l) \tag{48}$$

Higher values of turbulence velocity factor (u') would promote turbulent combustion at increased burn rates.

Another important design aspect of the ground electrode geometry is the shape of the joint between the ground electrode and the plug body. As is evident from Figure 24, the Pyrotek plug has a larger surface area compared with the baseline spark plug. It is possible that this increased area may also influence the bulk charge motion in its immediate vicinity in a manner favoring faster flame propagation. If the benefits of this effect outweigh the increased heat losses which might be incurred, this kind of joint might be advantageous. However, this aspect of spark plug shape was not studied in detail.

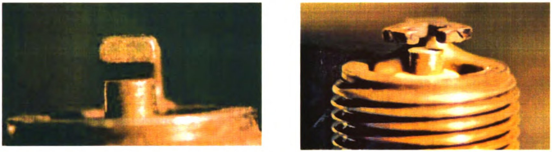

Figure 23: Ground Electrode Geometry

Figure 24: Ground Electrode Base

5.2 Effect of Ground Electrode Orientation

Since neither of the spark plugs are axisymmetric, their position with respect to the momentary flow direction influences the local flow field around the electrodes and thereby affects the fluid flow in the early stages of flame kernel growth. As the ground electrode orientation influences the velocity field within the spark-plug gap, it might facilitate early flame kernel convection either towards the ground electrode or away from the ground electrode, or neither, depending on the ground electrode orientation. The in-cylinder flow, the residual and inflow conditions, as well as intake system dynamics and cyclic variations in the flow field are strongly dependent on the inlet port, inlet valve, and cylinder head geometry. These flows appear to become unstable, either during the intake or compression process, and breakdown into three-dimensional turbulent motion. The jet-like character of the intake flow, interacting with the cylinder walls and piston motion creates large-scale rotating flow patterns within the cylinder [38] in some engines. Therefore, it is difficult to predict the path a flow might follow in the vicinity of a spark.

It is thought that the emissions produced by engines with spark plugs with larger and longer ground electrodes are more sensitive to the orientation of the spark plug [2]. This may be because larger ground electrodes generate broader wakes behind the electrode if the ground electrode faces the momentary flow direction. For spark plugs with smaller ground electrodes and shorter projections, engine emissions are not very sensitive to the flow direction [2]. The emissions measured with the Pyrotek spark plug were more sensitive to the ground electrode orientation than with the baseline Champion spark plug. A possible explanation for this observation is that the larger electrode area at the ground electrode base of the Pyrotek spark plug, shown at Figure 24, has a beneficial influence on the fluid motion in the vicinity of the spark gap which outweighs any disadvantages of increased heat loss.

The angular positions of the spark plug were denoted as 0° facing the exhaust valve, 90° facing the center of cylinder and 180° facing the intake valve, as shown in Figure 22. As noted by the Anderson and Asik [25], for a spark plug of baseline shape in a 0.4L Bowl- in-piston single cylinder engine, the 180° and 90° orientation have improved combustion performance over the 0° orientation. These results are consistent with our results using a baseline spark plug in a side valve engine. Anderson and Asik's explanation for the reduced performance as given in [25] is that: in the 0° orientation, the spark plug may shroud the gap from the charge motion. The electrode may create a recirculation region near the gap, which allows the charge a longer time for the formation of a stable flame kernel. In the 180° position, in contrast, it may allow the flow to move the flame kernel to regions where they experience increased contact with the electrode, greater heat losses reduced flame speed.

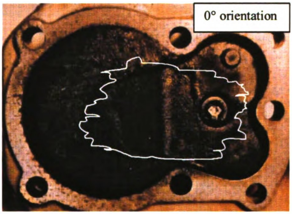

(a)

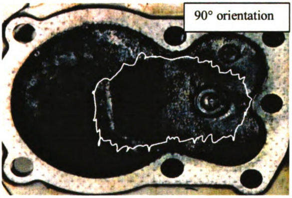

(b)

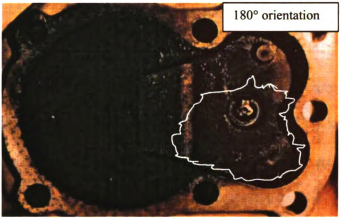

(c)

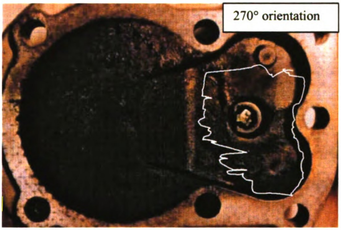

(d)

Figure 25: Cartoons of the Influence of Plug Orientation on Flame Front Shape

Another possible explanation for the improved performance of the Pyrotek spark plug may be the different ground electrode geometry. The ground electrode, when facing the exhaust valve (0° orientation), may cause the deflection of the any swirl flow in a manner inwhich the flame kernel is moved away from the electrode region toward the center of the combustion chamber, Figure 25(a). This may enhance its initial growth rate through reduced heat transfer to the electrode. The same effect may cause faster burning rates at 45°, 90° and 135° orientations. In the case of the ground electrode facing the inlet valve 180°, the larger shrouding effect cited by Anderson and Asik[25] may cause a longer residence time for flame kernel formation. This may cause excessive heat losses to the electrodes thus reducing the burning rates. The results obtained using the Pyrotek spark plug contradict the findings of Asik and Anderson [25] which were better for 180° orientation. However, they are in agreement are in agreement with the findings of Zeigler, Schaudt, and Herweg [26] for ignition in a constant flow chamber, which were better for the 0° orientation.

In the case of the idle runs, with the ground electrode facing the center of the cylinder (90°orientation), the unburned hydrocarbons were significantly lower than when the ground electrode was facing the nearest part of the cylinder wall (270°orientation). This might be explained if the local mean flow in the vicinity of the spark plug were toward the wall, thus blowing the flame kernel, on the average, towards the wall as shown in Figure (25d). Heat losses from the ensuing flame front to the wall may result in delayed combustion through this quenching effect. In addition, shrouding of the spark gap may also play a vital role in this configuration, causing more heat losses to the electrode surface. The hydrocarbon emissions of the baseline plug when facing the center and nearest part of the cylinder wall are scarcely different. This may be due to a reduction of Anderson and Asik's shrouding effect of the ground electrode of the baseline spark plug on flame kernel growth and charge motion.

In comparison with the findings of the other studies, the results obtained are in agreement with those of Zeigler, Schaudt, and Herweg [26] and Mantel [21] for the

Pyrotek spark plug, and with Anderson and Asik [25], in the case of the baseline spark plug. It appears, for a given bulk fluid motion, there exists an optimal spark plug orientation. However, the bulk fluid motions are often different at different engine speeds, loads, and throttle settings so a single optimization for a given engine may not always be possible.

5.3 Effect of Center Electrode Geometry

The center electrode of the Pyrotek spark plug was modified as shown in the Figure 26. In this case, a reduction in hydrocarbon emissions was achieved relative to the unmodified Pyrotek and base line spark plugs. The disadvantage of an unnecessarily large electrode area, compared with the baseline spark plug, was partially overcome by making a V-notch in the center electrode. Based on experimental observations that spark discharge occurred mainly at the periphery of the center electrode, the flame kernel contact area can be reduced by reducing the effective surface area of the center electrode. In the flame growth phase, convective heat loss plays an important role, as modeled as

$$\dot{Q}_{loss} = hA_c(T_b - T_l), \tag{49}$$

where A_c is the contact area with the electrodes. The contact area fraction can be used to estimate the effect of heat loss to the electrode during flame growth. As noted in [24], this contact area fraction is lower for the thin electrodes when using spark plugs of baseline design.

The *HC* emissions results of Chapter 4 show that plugs with smaller contact area yield greater benefits at idle and low loads. This observation is also consistent with the findings of Hood [4]. Since this engine was operating at an equivalence ratio of roughly 1.3, where Heywood [24] has noted that these heat transfer effects are not as significant as at leaner mixtures, the potential benefits of the V-notch geometry might be even greater at equivalence ratios closer to 1.

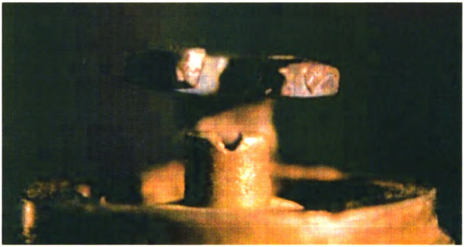

Figure 26: Center Electrode Geometry

5.4 Effect Of Spark Gap

The influence of the spark gap manifests itself through two effects. The first effect is to change the breakdown voltage and energy discharged: the larger is the gap, the higher is the voltage required to break down the gap, and the larger the energy released in this phase of discharge. The second effect is to change the proportion of energy lost to the electrodes through heat transfer.

It was observed that emissions measured using Pyrotek spark plugs were more sensitive to the spark gap than those using a baseline plug. A plausible explanation is: for small gaps, the electrodes remove excessive quantities of heat from the incipient flame, thus causing a reduction in the flame propagation speed and therefore increasing the burn duration. This effect seems to be more pronounced when there is a large contact area, as with the Pyrotek ground electrode.

As the spark gap is increased above the recommended value, the flame has more room to grow without the influence of the electrodes. However, when the spark gap becomes too wide, a higher voltage is required across the gap, the energy release rate become faster and the spark duration become smaller. The spark may lose excessive energy to the unburned mixture through heat transfer. Increasing the spark gap also requires higher breakdown voltages with associated reductions in the spark duration. This reduced spark duration slows flame kernel growth [12] resulting in higher HC emissions.

5.5 Effect of engine rpm on comparative emissions of two spark plugs

When fitted with the Pyrotek spark plug, hydrocarbon emissions decreased almost linearly with increasing engine speed. In contrast, emissions of this engine equipped with the baseline spark plug rise to a maximum at 2600 rpm and then decrease at higher engine speeds. The differences in these responses can be attributed to the differences in spark-plug geometry. A possible interpretation is that each electrode may influence bulk gas motions in the vicinity of the spark-plug gap differently, which is consistent with the findings of Halldin [38]. It is also related to the observation of Witze, Hall and Bennett [34], that the swirl velocity increases linearly with engine speed, which might cause a proportional increase in the flame kernel growth rate. Shen and Jiang [35] also studied this effect by comparing the early flame kernel development at different engine speeds, and noticed that turbulence intensity varies almost linearly with the mean piston velocity.

Chapter 6

Conclusions

1. The Pyrotek spark-plug ground-electrode geometry changed the emission characteristics of several small engines compared to baseline Champion spark plugs.

2. Use of the Pyrotek spark plug caused reductions in *HC* emissions from these engines which were attributed primarily to faster flame kernel growth rates. The faster flame kernel growth rates were attributed to the larger initial flame kernels produced by the Pyrotek spark plug over a larger effective gap.

3. A secondary effect of the Pyrotek geometry was thought to favor the faster initial flame-kernel growth by enhancing convection of the initial flame kernel away from the electrodes, thereby reducing the heat losses.

4. At low loads, the benefits of the Pyrotek electrode may be outweighed by higher heat losses to the electrodes. This can be partially overcome by reducing the center electrode contact area.

5. The Pyrotek spark plug is more sensitive to its ground electrode orientation when compared to the baseline spark plug. This is attributed to the effect of the larger

surface area in promoting heat transfer and the shape of Pyrotek spark plug electrode on the local flow field.

6. There exists an optimum spark gap and ground electrode orientation for each combustion chamber geometry and engine operating conditions.

Appendix

Appendix A

Factors Effecting Burn Duration

A.1 Engine speed

Mixture burning rate is strongly influenced by the engine speed. Burning rate throughout the combustion process increases almost as rapidly as engine speed, increasing in-cylinder velocities. This increase in burn duration due to the increased in-cylinder velocities causes an increase in the turbulent intensity, resulting in more turbulent combustion.

A.2 Equivalence ratio

The influence of the equivalence ratio is small for near stoichoimetric mixtures in the range as $0.8 < \phi < 1.2$. The burn duration increases with larger deviations from stoichiometry due to the decrease in the laminar speed or equivalently the reaction rate. The burn duration varies significantly less over the same range of air fuel ratios if the spark timings are varied, such that combustion takes place closer to the TDC. This indicates that the increase is mainly caused by the initial combustion process where the laminar speed is important. The increase in the burn duration is determined from the influence of chemical kinetics and is more pronounced at low levels of turbulence.

A.3 Flow field effects

Flow field effects can be divided into small-scale effects and the large-scale effects. The small-scale effects are local in nature, such as the local turbulence levels, air fuel ratio fluctuations, and heat transfer rates. These small-scale effects are highly influenced by the large-scale effects, such as mean flow structures, geometry, and overall fuel ratio. The turbulence, for instance, enhances the local flame propagation, but the mean flow structures effect the total front area and the flame position within the combustion chamber. The total combustion duration is determined by the combined effect of propagation speed and necessary flame travel distances to burn up the charge. The best performance is obtained when both the small-scale structure and the large-scale structure are more favorable for the combustion process. The concept of using both large-scale and small-scale flow to promote the combustion has already been implemented. Fast burn engines have shown improvement in the fuel consumption and a control of emissions [28].

A.4 Effect of swirl and tumble

Swirl and tumble also influence burn duration. Experiments have revealed that engine with high swirl and tumble had a faster burn rate as compared to those with quiescent flow in every stage of the combustion [18]. The greatest improvement on account of tumble occurs at the early part of the cycle whereas in the case of swirl the burn rate improvement is in the middle of the burning process. As reported by [18], when tumble is present, the organized motion is broken up into small-scale turbulence during the compression process so that the turbulence intensity is highest at the end of compression. In the case of swirl, although the swirl velocity decays somewhat during the compression and expansion, the magnitude of the mean velocity and turbulence remains reasonably high, and the burn rate is sustained until later in the cycle.

Appendix B

Factors Effecting the Flame Kernel Growth

B.1 Ignition energy and spark duration

The three phases of ignition process [20] are: the breakdown phase, the arc phase, and the glow phase. The break down phase was found to have high thermal efficiency. In addition, ignition systems with longer spark durations (1.5 - 2 ms) are also very efficient, because they permit the maintenance of a hot central core. From this hot kernel core, heat may diffuse to the flame surface and mask cycle to cycle variations near the spark gap.

The lengthening of the spark discharge duration is particularly effective in achieving stabilized combustion [12]. Longer spark duration provides a continued supply of electrical energy as kinetic energy to the mixture around the spark gap. Analytical results and constant volume combustion chamber tests verify that longer spark duration promotes flame initiation and makes more reliable flame propagation possible [12]. The length of the spark duration is regarded as the period from ignition to the onset of combustion pressure rise.

B.2 Effect of electrical energy on flame growth

Based on experimental observations [6], the cycles in which the flame kernel is convected away from the electrodes are more likely to be the cycles with more electrical energy transferred to the kernel. The discharge channel follows the flow field and is stretched in length leading to a larger voltage drop in the positive column, which implies that the higher electrical energy leads to a fast initial flame growth. The cycles with larger flame radii are the cycles, which result in earlier 10% burned location, indicating faster flame kernel growth rate.

B.3 Heat losses to spark plug electrodes

Generally, the presence of the electrodes can be described as a heat or radical sink, which can eventually lead to the "flame quenching" in the case of unsuccessful ignition. The flame kernel and electrode geometry play a significant role in the heat transfer from the flame kernel to the electrodes. The character and relevance of the geometrical interactions between flame and electrode are of particular interest in an engine, where the flame development process is known to vary from cycle to cycle. The influence of this heat transfer from the flame kernel to the electrodes greatly depends on the contact area ratio. The electrodes with smaller area are found to have smaller heat losses thus resulting in better combustion [24].

B.4 Flame kernel advection

It has been observed experimentally that smaller flame kernel are essentially centered in the spark gap whereas larger flame kernels are convected away from the spark gap center. As observed by the Heywood [24], there exists a correlation between the flame radius and the flame kernel displacement. Flame kernels, which are convected away from the gap center, grows faster. The cycles in which flame kernels do not move away from the electrodes, have slower growth. The basic cause of this phenomenon is heat losses from the flame kernel to the electrodes.

B.5 Characteristics of charge motion

The flame initiation is accelerated when the flow field convects the initial flame kernel. Cycle to cycle analyses [24] of flame initiation have shown that a flow velocity at the ignition point is favorable to succesful initiation. When the flame kernel is convected away from the electrode gap, the heat losses to the electrode wall are limited. The secondary effect of the flow is to stretch of initial flame. The characteristics of the charge motion have a significant effect on the expansion velocity. The expansion velocity is enhanced by an increase in the entrainment area due to the wrinkling of the flame front by the turbulence. In addition, the flame front may be stretched considerably if the flame kernel is 'anchored' at the spark gap when there is substantial bulk motion.

B.6 Effect of convection velocity

The overall convection of the flame kernel in the early stages of flame development is due to the bulk charge motion at the spark plug. This bulk flow could move the flame kernel away or toward the electrodes and change the heat losses from the flame. The high bulk flow would also lengthen the discharge channel and would increase the electrical energy to the kernel. In addition, the direction of the flame kernel toward or away from the wall also influences the flame geometry relative to the combustion chamber at the later stages of flame development. There is a strong correlation which exists between the expansion speed and the flame kernel convection velocity. This correlation can be explained by three factors

- Turbulent velocity fluctuations are higher, if the bulk charge motion velocity is higher, hence there is a faster flame due to the turbulent enhancement of the flame speed.
- For 'anchored' flames, the higher convection velocity gives a larger flame stretch.
- Higher convection velocities tends to advect the flame kernel out of the spark plug region, hence reducing the heat losses to the spark plug electrodes. [24].

Appendix C

Engine Data:

Table 3: Two Stroke Chainsaw Engine

Bore (cm)	3.642
Stroke(cm)	3.12
Displacement(cm^3)	32.4
Rated kW	1
Configuration	two stroke

Table 4: Four Stroke Tecumseh Side Valve (VLV60) Engine

Bore (cm)	7.1018
Stroke(cm)	5.1993
Displacement(cm^3)	207
Rated kW	4.4742
Configuration	vector light weight vertical (side valve)

Table 5: Four Stroke Tecumseh Overhead Valve (OHH50) Engine

Bore (cm)	6.6675
Stroke(cm)	4.92252
Displacement(cm^3)	171.89963
Rated kW	3.7285
Configuration	Overhead valve Horizontal

Appendix D

Overview of Emission Bench and Dynamometer

D.1 Dynamometer

The Hydraulic dynamometer dissipates the energy produced by the engine through an oil to air heat exchanger. It uses a hydraulic pump driven by an electric motor. The flow rate is controlled by the computer via a stepper motor, which governs the engine RPM. The RPM are set by the flow rate with the use of Stepper motor and the engine can be loaded to desired setting while rpm is kept constant. A torque sensor is mounted between the engine and the hydraulic pump to monitor the torque loading of the engine.

D.2 Emission Measurements

D.2.1 *CO* and CO_2 measurements

The *CO* and CO_2 meters employ a non-destructive measurement technique. This involves passing a specific wavelength of infrared light (IR) through the sampled gas. An IR detector on the opposite side detects how much IR light has passed through the sample. Since *CO* and CO_2 absorb the IR light (over different frequency ranges), the greater the concentration of CO or CO_2 in the sample, the less IR light that will pass through.

D.2.2 *HC* measurements

The *HC* meter uses a different approach and is tuned to specific carbon compositions within hydrocarbon mixtures. Composition of the two stroke exhaust will mirror the composition of the two stroke fuel whereas, the composition of the four stroke exhaust is mostly C_1 and C_2 molecules [33]. Therefore, a span gas is used which it closely resembles the exhaust gas in question. The analyzer detects the amount of the *HC's* present in the sample using the flame ionization technique. The flow of a sample with carbon compounds through the hot flame leads to an ionization current. This current is proportional to the volume fraction of the *HC's* present within the sample.

D.2.3 NO_x measurements

The NO_x meter uses a chemical illumenescent process. Nitrogen compounds in the exhaust gas are actually a mixture of NO and NO_2, which are usually written NO_x. In the analyzer, the NO_2 is first converted to NO. The resulting sample then react with O_3, which is generated by an electric discharge through the oxygen, at a low pressure in a heated vacuum chamber. The light emitted by the reaction is measured by a photo-multiplier and indicates the NO_2 concentration within the converted sample.

Appendix E

Experimental results in tabulated data form

E.1 Ground electrode geometry

E.1.1 Two Stroke Chain Saw Engine

TABLE 6: Effect of Three Different Spark Plug on Two Stroke Engine Characteristics

Spark Plug	Pyrotek	New(base)	Used(base)	Pyrotek	New(base)	Used(base)
Parameters	6%	6%	6%	100%	100%	100%
Power(Brake Hp)	0.05	0.05	0.04	0.84	0.81	0.74
Torque(Ft_Lb)	0.06	0.06	0.05	0.46	0.44	0.41
Exht Temp(C°)	214.10	224.80	212.60	393.03	398.93	385.33
CO (grms/hour)	8.00	56.50	60.60	680.30	716.83	687.67
CO_2 (grms/hour)	229.98	224.46	212.27	870.52	806.01	745.74
NO_x (grms/hour)	0.00	0.00	0.00	0.63	0.47	0.47
HC (grms/hour)	31.03	32.70	34.12	203.08	229.99	237.72
AFR	14.26	8.87	8.82	11.77	12.86	12.92
RPM	4340.00	4433.00	4573.00	9571.00	9537.33	9521.67

E.1.2 Four Stroke Tecumseh Sidevalve (VLV60) Engine

TABLE 7: Effect of Ground Electrode Geometry on Four Stroke Engine Emissions

Parameters		Idle	10%	25%	50%	75%	WOT
Power(Brake Hp)	Baseline	0.00	0.34	0.66	1.43	2.25	2.90
	Pyrotek	0.00	0.36	0.72	1.37	2.19	2.91
Torque(Ft_Lb)	Baseline	0.00	0.92	1.27	2.73	4.22	5.47
	Pyrotek	0.00	0.81	1.36	2.58	4.13	5.47
Temp Exht(C°)	Baseline	153.97	274.17	317.70	310.23	376.50	370.47
	Pyrotek	233.67	281.37	292.17	345.80	375.87	373.67
CO (grms/hour)	Baseline	150.03	5.40	68.30	284.33	586.43	1235.87
	Pyrotek	5.97	76.73	224.00	23.47	539.90	1338.30
CO_2 (grms/hour)	Baseline	209.70	616.06	864.73	964.67	1559.02	1438.42
	Pyrotek	441.53	693.73	831.97	1224.38	1536.14	1395.39
NO_x (grms/hour)	Baseline	0.03	0.90	1.47	3.07	19.40	3.47
	Pyrotek	0.67	0.60	1.03	10.53	19.67	2.83
HC (grms/hour)	Baseline	16.13	5.59	7.10	9.56	13.91	20.23
	Pyrotek	17.70	6.67	6.83	4.53	12.74	22.35
AFR	Baseline	9.69	14.07	13.55	11.72	11.83	10.22
	Pyrotek	12.83	13.26	12.36	14.21	11.95	9.98

E.1.3 Four Stroke Tecumseh Overhead Valve (OHH50) Engine

TABLE 8: Effect of Ground Electrode Geometry on Overhead Valve Engine

Parameters		Idle	10%	25%	50%	75%	WOT
Power(Brake Hp)	Baseline	0.00	0.36	0.85	1.81	2.62	3.41
	Pyrotek	0.00	0.35	0.89	1.79	2.60	3.40
Torque(Ft_Lb)	Baseline	0.00	0.67	1.60	3.41	4.92	6.41
	Pyrotek	0.00	0.66	1.67	3.38	4.89	6.38
Temp Exht(C°)	Baseline	112.73	188.03	221.53	279.67	339.33	374.50
	Pyrotek	111.70	184.57	218.83	278.43	337.03	367.67
CO (grms/hour)	Baseline	169.40	239.00	167.90	70.53	371.37	595.57
	Pyrotek	169.83	243.30	162.07	76.90	367.57	583.00
CO_2 (grms/hour)	Baseline	204.52	652.08	875.43	1441.62	1546.16	1872.56
	Pyrotek	203.00	623.97	881.69	1438.99	1535.31	1872.22
NO_x (grms/hour)	Baseline	0.03	0.60	1.40	13.90	13.77	11.77
	Pyrotek	0.07	0.50	1.50	14.43	14.13	12.47
HC (grms/hour)	Baseline	28.28	7.28	5.07	4.36	6.90	6.64
	Pyrotek	28.00	6.69	4.78	4.17	6.62	5.93
Fuel(grms/hour)	Baseline	522.57	436.67	538.97	669.77	837.70	960.13
	Pyrotek	408.40	457.20	509.13	585.80	825.37	959.57
AFR	Baseline	8.81	11.82	12.86	13.98	12.61	12.23
	Pyrotek	8.81	11.73	12.92	13.95	12.62	12.27

E.2 Effect Of Ground Electrode Orientation

TABLE 9: Effect of Ground Electrode Geometry (Pyrotek) Spark Plug at Part Load

Orientation	0°	45°	90°	135°	180°
Power(Bhp)	1.30	1.27	1.27	1.24	1.23
Torque(Ft-Lb)	2.41	2.34	2.34	2.30	2.28
Exhaust Temp (C°)	294.80	304.90	298.40	298.73	294.20
CO(gms/hr)	349.93	362.76	368.56	360.66	359.36
HC (gms/hr)	9.18	9.36	9.88	9.39	10.18
CO_2(gms/hr)	931.19	902.50	903.85	860.47	881.78
NO_x(gms/hr)	1.87	1.73	1.73	1.66	1.76
AFR	11.81	11.68	11.65	11.66	11.64

TABLE 10: Effect of Ground Electrode Geometry (Baseline) Spark Plug at Part Load

Orientation	0°	90°	180°
Power(Bhp)	1.2420	1.2500	1.2430
Torque(Ft-Lb)	2.3000	2.3140	2.2940
Exhaust Temp (°C)	288.7300	295.0000	889.3000
CO(gms/hr)	353.7600	350.5000	350.1300
$HC's$(gms/hr)	9.2900	8.9600	8.8200
CO_2(gms/hr)	876.5000	886.1160	888.1400
AFR	11.6800	11.7200	11.7300

TABLE 11: Effect of Ground Electrode Geometry (Pyrotek) at Idle

Orientation	270°	90°
RPM	1975	1933
Exhaust Temp (°C)	118	136.6
CO(gms/hr)	106.6	170
HC's(gms/hr)	71.46	36.84
CO_2(gms/hr)	243.6	275.7

TABLE 12: Effect of Ground Electrode Geometry (Baseline) at Idle

Orientation	270°	90°
RPM	1709	1574
Exhaust Temp (°C)	107.8	121.7
CO(gms/hr)	82.5	126.13
HC's(gms/hr)	63.67	52.77
CO_2(gms/hr)	223.14	242.936

E.3. Effect Of Center Electrode Geometry

TABLE 13: Effect of Center Electrode Geometry (V-Notch) on Emissions

Parameters		Idle	10%	25%	50%	75%	W O T
Power(Brake Hp)	Baseline	0.00	0.41	0.87	1.80	2.51	3.55
	Pyrotek	0.00	0.36	0.91	1.78	2.47	3.40
	V-Groove	0.00	0.30	0.87	1.84	2.62	3.59
Torque(Ft_Lb)	Baseline	0.00	0.77	1.64	3.39	3.14	6.69
	Pyrotek	0.00	0.68	1.71	3.35	4.65	6.46
	V-Groove	0.00	0.57	1.64	3.46	4.87	6.74
Temp Exht('C)	Baseline	122.70	183.93	218.87	281.97	332.07	394.20
	Pyrotek	121.03	184.30	215.07	275.17	328.57	385.97
	V-Groove	127.80	181.83	215.33	279.37	330.80	392.53
CO (grm/hr)	Baseline	218.73	380.43	170.20	120.07	286.57	580.47
	Pyrotek	217.20	377.70	170.40	117.17	267.40	573.27
	V-Groove	216.07	359.73	146.47	122.80	274.33	575.17
CO_2 (grm/hr)	Baseline	464.26	616.06	895.03	1330.98	1595.46	1845.12
	Pyrotek	435.80	616.23	883.91	1313.54	1569.87	1773.51
	V-Groove	477.07	608.56	940.89	1342.27	1577.12	1842.39
NO_x (grm/hr)	Baseline	0.10	0.40	1.60	13.13	18.30	11.27
	Pyrotek	0.10	0.40	1.70	13.53	18.73	10.73
	V-Groove	0.10	0.40	1.80	14.17	19.53	11.47
HC (grms/hour)	Baseline	16.00	11.30	5.63	6.29	7.53	9.96
	Pyrotek	15.80	11.06	5.32	6.07	7.36	8.74
	V-Groove	13.73	10.22	3.54	5.94	7.14	8.58
AFR	Baseline	10.95	10.79	12.85	13.58	12.96	12.20
	Pyrotek	10.83	10.81	12.84	13.59	13.02	12.17
	V-Groove	11.12	10.89	13.15	13.58	13.01	12.23

E.4. Influence of Spark Gap on Emissions

TABLE 14: Influence of Different Spark Gaps on Engine Emissions

Gap	0.0025	0.003	0.0035	0.004	0.0045
Baseline-HC (gms/hr)	9.62	9.43	9.13	10.55	10.12
CO(gms/hr)	407.60	430.57	420.43	445.37	442.90
CO2(gms/hr)	883.37	874.90	836.87	837.47	866.57
Exht Temp (°C)	297.67	293.43	307.70	282.67	290.80
Pyrotek-HC (gms/hr)	10.53	9.26	10.14	10.83	10.64
CO(gms/hr)	444.87	421.15	432.70	446.63	441.80
CO2(gms/hr)	890.36	859.43	874.56	832.52	870.77
Exht Temp (°C)	234.80	302.47	248.83	286.63	306.03

E.5. Effect of Engine Speed on Emissions

TABLE 15: Effect Of Engine Rpm On Exhaust Emissions With Pyrotek Spark Plug

Rated RPM	2400	2600	2800	3000
Power(BHP)	1.385	1.452	1.460	1.408
Torque(ft-lb)	3.046	2.942	2.745	2.470
CO(gms/hr)	11.267	19.100	31.100	33.567
CO_2(gms/hr)	1156.507	1221.033	1273.327	1311.527
NO_x(gms/hr)	14.000	13.367	11.233	8.700
$HC's$(gms/hr)	4.760	4.587	4.120	4.020
Exhaust Temp (°C)	246.367	256.400	258.900	263.667
AFR	14.28	14.24	14.18	14.18
NO_x(gms/hp/hr)	10.067	9.233	7.733	6.200
$HC's$(gms/hp/hr)	3.437	3.160	2.823	2.853

TABLE 16: Effect of Engine RPM On Exhaust Emissions With Baseline Spark Plug

Rated RPM	2400	2600	2800	3000
Power(BHP)	1.35	1.42	1.40	1.29
Torque(ft-lb)	2.97	2.88	2.64	2.26
CO(gms/hr)	13.60	21.87	24.07	30.70
CO_2(gms/hr)	1155.24	1222.36	1308.60	1324.97
NO_x(gms/hr)	11.83	11.50	9.80	7.77
$HC's$(gms/hr)	4.75	5.16	4.38	3.54
Exhaust Temp (°C)	252.73	259.73	266.20	269.57
AFR	14.26	14.20	14.23	14.22
NO_x(gms/hp/hr)	8.77	8.10	6.97	6.00
$HC's$(gms/hp/hr)	3.51	3.63	3.12	2.75

APPENDIX F

Effect of Use of Indexing Washers on Compression Ratio

Engine Data:

Displacement = 10.49 in^3

Stroke = 1.938 in^3

Bore = 2.625 in^3

$V_1 = (\pi/4)\, D^2\, l$ = 10.48823 in^3

Given $\gamma = 7.5 = (V_1 + V_2)/\, V_2 \quad \Rightarrow V_2$ = 1.613573 in^3

One turn of spark plug is equal to the 0.050-inch washer if turned in or turned out.

By measurements:

OD of spark plug = 0.5435 inch

ID of spark plug = 0.336 inch

Then $\Delta V = \pi/4\ \{(0.5435)2 - (0.336)2\ \} * 0.050 = 7.1666 * 10^{-3}$ $inch^3$

If we turn in the spark plug by one complete turn then the new compression ratio would be:

New compression ratio = $(V_1 + V_2 - \Delta V)/ (\ V_2 - \Delta V)$ = 7.5289

Percentage change in compression ratio 0.386 %

For ½ or ¼ turn, the effect would be much smaller.

LIST OF REFERENCES

LIST OF REFERENCES

1. Milton, B. E., "Thermodynamics, Combustion and Engines," Chapman and Hall, First edition, 1995.

2. Danials, C, F., Scilzo, B, M., " The Effect of Electrode Design on Mixture Igniteability," SAE paper 960606, 1996.

3. Nishio, K., Oshima, T., Sher, E., "Cyclic Variability In Spark Ignition Engines, A Literature Survey," SAE Paper 940987, 1994.

4. Hood, S., " The V-Groove Electrode Spark Plug," SAE paper 901535,1990.

5. Hadjiconstatinou, N,. Min, K., Heywood, J. B., "Relation Between Flame Propagation Characteristics and Hydrocarbon Emissions Under Lean Operating Conditions in Spark Ignition Engines," Twenty Sixth Symposium (International) on Combustion/ The Combustion Institute, 1996(PP 2637-2644).

6. Bianco, Y., Cheng, W, K., Heywood, J. B., " The Effect Of Initial Flame Kernel Conditions on Flame Development In SI Engines," SAE paper 912402, 1991.

7. Witze, P, O., " The Effect Of Spark Location On Combustion In A Variable Swirl Engine" SAE paper 820044,1982.

8. Herweg, R., Begleris, P., Zettlitz, A., and Zeigler, G, F, W., " Flow Field Effect On Flame Kernel Formation In A Spark Ignition Engines," SAE paper 881639, 1988.

9. Hall, M.J., " The Influence of Fluid Motion on Flame Kernel Development And Cyclic Variation In A Spark Ignited Engine," SAE paper 890991, 1989.

10. Anbarasu, A. M., and Abata, D. L., " Modeling of Heat Loss to the Spark Plug During Early Flame Growth in A Spark Ignition Engine," ICE-Vol 23, Engine modeling, ASME 1995.

11. Maly, R., Saggau, B., Wagner, E., and Zeigler, G., " Prospects of Ignition Enhancement," SAE paper 830478, 1983.

12. Nakai, M., Nakagawa, Y., Hamai, K., Sone, M., " Stabilized Combustion in A Spark Ignited Engine Through A Long Spark Duration," SAE paper 850075, 1985.

13. Brereton, G. J., Bertrand, E., and Macklem, L., " Effect Of Changing Ambient Humidity And Temperature On The Emissions Of Carbureted Two And Four Stroke Hand Held Engines," SAE paper 972707, 1997.

14. Turns, S. R., " An Introduction To Combustion: Concepts And Applications," Mcgraw Hill , First Edition , 1996.

15. Gaydon, A. D., and Wolfhardt, H. G., " Flames, Their Structure , Radiation and Temperature," Chapman and Hall, Ltd., London, 1970.

16. Fraser, R. A., and Bracco, F. V., "Cycle Resolved LDV Integral Length Scale Measurements In An ICE Engine," SAE paper 880381,1988.

17. Chen, C., and Veshagh, A., "A Refinement of Flame Propagation Combustion Model for Spark-Ignition Engines," SAE Paper 920679.1992.

18. Lancaster, D. R., Krieger, R. B., Sorenson, S. C., and Hull, W. L., "Effect of Turbulence on Spark Ignition Engine Combustion," SAE paper 760160,1976.

19. William, F. A., " Combustion Theory," Second Edition, Addison- Wesley, Redwood City, CA, 1985.

20. Maly, R. R., " Spark Ignition, its Physics and Effects on the Internal Combustion Engine," Fuel Economy In Road Vehicles Powered By Spark Ignition Engines, Hilliard and Springer, G. S., Plenum Press, 1983.

21. Mantel, T., " Three Dimensional Study Of Flame Kernel Formation Around A Spark Plug," SAE paper 920587, 1992.

22. Kanury, A. M., " Introduction to Combustion Phenomena," Combustion Science and Technology, Volume 2, Gordon and Breach Science Publishers, 1984.

23. Bertrand, E. C., "Effect Of Ambient Conditions of A Small Carbureted Overhead Valve Four Stroke Utility Engine," Master Thesis, 1997.

24. Heywood, J. B., and Pischinger, S., " How Heat Losses to the Spark Plug Electrodes Affect Flame Kernel Development In An SI Engine," SAE paper 900021, 1990.

25. Anderson, R. W., and Asik, J. R., " Ignitability Experiments in a Fast Burn, Lean Burn Engines," SAE paper 830477,1983.

26. Ziegler, G. F. W., Schaudt, R. A., and Herweg, R., " The Influence of Spark Plug Orientation On Flame Kernel Formation in Flowing Mixtures," SAE paper 865031,1986.

27. De Soete, G. C., " Propagation Behavior of Spark Ignited Flames in Early Stages," C-59/83.

28. Mattavi, J. N., and Amann, C. A., " Combustion Modeling in Reciprocating Engines," Plenum, Newyork, 1980.

29. Hacohen, J., Yossafi, D., Thomas, J., Thurly, R., Belmont, M.R., " Flame Stretch and Heat Transfer Effects During Flame Initiation in SI Engines," American Chemical Society Paper 93359, 1993.

30. Markstein, G H., " Non Steady Flame Propagation," Pergamon, New York, 1964.

31. Metaghalchi, M., Keck, J.C., " Burning Velocities of mixture of air with methanol, Isooctane, and Indolene at high Pressure and Temperatures," Combustion and Flame, 48; 1982.

32. Lefebvre, A. H., " Gas Turbine Combustion," McGraw-Hill, 1983.

33. Eccleston, B. H., Hurn, R.. W., " Exhaust Emissions from Small Utility Internal Combustion Engines," SAE Paper 720197, 1972.

34. Witze, P.O., Hall, M. J., Bennet, M. J., "Cycle Resolved Measurements of Flame Kernel Growth and Motion Correlated with Combustion Duration," SAE Paper 900023, 1990.

35. Shen, H., Jiang, D., " Investigation on the Flame Initiation and Early Development in a Spark Ignition Engine," SAE Paper 922239, 1992.

36. Semenev, E. S., "Studies of the Turbulent Gas Flow in Piston Engines," NASA Technical translation F-97, 1963.

37. Spindt, R. S., "Air Fuel Ratios from Exhaust Gas Analysis," SAE Paper 650507,1965.

38. Halldin, C., " Velocity and Turbulence Measurements Close to a Spark Plug," SAE Paper 920154, 1992.

39. Heywood, J, B., "Internal Combustion Engine Fundamentals," McGraw-Hill, 1988.

40. Wichman, I. S., "Introduction to Combustion" Course Notes, 1997.

41. Brown, A. G., Stone, C. R., Beckwith, P., "Cycle-by-Cycle Variations in Spark Ignition Engine Combustion- Part 1: Flame Speed and Combustion Measurements and a Simplified Turbulent Combustion model," SAE Paper 960612, 1996.